Medical Image Analysis 32 (2016) 46–68

Contents lists available at ScienceDirect

Medical Image Analysis

journal homepage: www.elsevier.com/locate/media

Survey Paper

Reconstruction of coronary arteries from X-ray angiography: A review☆

Serkan Çimen[a,*], Ali Gooya[a], Michael Grass[b], Alejandro F. Frangi[a]

[a] Department of Electronic and Electrical Engineering, University of Sheffield, Sheffield S1 3JD, United Kingdom
[b] Philips Research, Röntgenstraße 24-26, 22335 Hamburg, Germany

ARTICLE INFO

Article history:
Received 18 September 2015
Revised 29 January 2016
Accepted 22 February 2016
Available online 11 March 2016

Keywords:
Review
X-ray angiography
Coronary artery reconstruction
Modelling
Tomographic reconstruction

ABSTRACT

Despite continuous progress in X-ray angiography systems, X-ray coronary angiography is fundamentally limited by its 2D representation of moving coronary arterial trees, which can negatively impact assessment of coronary artery disease and guidance of percutaneous coronary intervention. To provide clinicians with 3D/3D+time information of coronary arteries, methods computing reconstructions of coronary arteries from X-ray angiography are required. Because of several aspects (e.g. cardiac and respiratory motion, type of X-ray system), reconstruction from X-ray coronary angiography has led to vast amount of research and it still remains as a challenging and dynamic research area. In this paper, we review the state-of-the-art approaches on reconstruction of high-contrast coronary arteries from X-ray angiography. We mainly focus on the theoretical features in model-based (modelling) and tomographic reconstruction of coronary arteries, and discuss the evaluation strategies. We also discuss the potential role of reconstructions in clinical decision making and interventional guidance, and highlight areas for future research.

1. Introduction

Coronary artery disease (CAD), also known as coronary heart disease, is a serious illness, which is responsible for 1 of every 5 deaths in Europe (Nichols et al., 2013) and 1 of every 6 deaths in US (Go et al., 2014). In addition to the severe mortality rates, the direct and indirect costs associated with CAD are major burdens on healthcare systems (Nichols et al., 2013; Go et al., 2014). Early diagnosis of CAD, effective prognostic markers of treatment outcome, and the availability of minimally invasive treatment options for CAD have all motivated steady progress in diagnostic and interventional imaging modalities to quantify the anatomy and function of the coronary arteries.

Current clinical practice for assessing the presence and the extent of the CAD relies on medical imagery acquired through various diagnostic (cardiac computed tomographic angiography (CCTA) (Kachelriess et al., 2000; Shechter et al., 2003b; Mark et al., 2010) and magnetic resonance angiography (MRA) (Stuber and Weiss, 2007)) and interventional (invasive X-ray coronary angiography (Sones and Shirey, 1962; Klein and Garcia, 2009)) imaging modalities. Other hybrid imaging modalities such as intravascular ultrasound (IVUS), optical coherence tomography (OCT) (Hetterich et al., 2010) can be used diagnostically, but require an intervention. Apart from their diagnostic role, these imaging modalities also help clinicians to select between therapeutic options and plan interventional procedures.

Invasive (catheter-based) X-ray coronary angiography is one of the most commonly utilised method to assess CAD and is still considered the gold standard in clinical decision making and therapy guidance (Mark et al., 2010). This imaging modality is based on the radiographic visualisation of the coronary vessels with injection of a radiopaque contrast material (Scanlon et al., 1999).

Although X-ray coronary angiography has drastically evolved since its first introduction five decades ago, it is known to be fundamentally limited in some aspects (Green et al., 2004; Carroll et al., 2009). X-ray coronary angiography represents complex 3D/4D (3D+time) structure of the contrast filled coronary arteries by 2D X-ray projections or silhouette images, which can be degraded by imaging artifacts (Green et al., 2004). A considerable amount of 3D/4D information of the coronary arteries is lost due to the consequences of the projection operation. Specifically, the cumulative effect of suboptimal projection angles, vessel overlap, foreshortening, tortuosity and eccentricity may all lead to underestimation of stenoses severity and incorrect stent size selection (Green et al., 2004).

In order to obviate the fundamental limitation of X-ray coronary angiography described above, a 3D/4D description of the coronary

☆ This paper was recommended for publication by Nicholas Ayache.

* Corresponding author.
E-mail addresses: s.cimen@sheffield.ac.uk (S. Çimen), a.gooya@sheffield.ac.uk (A. Gooya), michael.grass@philips.com (M. Grass), a.frangi@sheffield.ac.uk (A.F. Frangi).

http://dx.doi.org/10.1016/j.media.2016.02.007
1361-8415/

arterial tree may be reconstructed from the 2D projection images. This inverse problem of reconstruction is known to be ill-posed and it entails some additional challenges in the context of X-ray coronary angiography. These challenges include: intensity inhomogeneities due to blood flow inside the arteries, overlap of different structures (e.g. catheters, bones), and more importantly respiratory and cardiac motions (Cardenes et al., 2012). These challenges are addressed in different manners depending on the type of X-ray coronary angiography.

Thanks to the advances in the C-arm based angiography systems in the cardiac catheterization laboratory (cath-lab), various kinds of X-ray coronary angiography exists, namely single plane (standard/conventional), biplane, rotational and dual-axis rotational coronary angiography (DARCA). The diversity of the X-ray coronary angiography strategies inevitably leads to the diversity of the 3D/4D reconstruction algorithms, because different strategies necessitate special considerations for the reconstruction algorithms.

In this review, we focus on the 3D/4D reconstruction of coronary arteries from invasive X-ray coronary angiography. The most recent reviews (Chen and Schäfer, 2009; Schoonenberg et al., 2009a) about coronary artery reconstruction provide a good overview of the subject but are partial reviews of the topic. In this review, we follow the taxonomy proposed by Chen and Schäfer (2009), Schoonenberg et al. (2009a), and divide the literature into two main categories, dealing with model-based methods (modelling) and tomographic reconstruction aspects. Model-based methods try to find a binary representation of the 3D/4D structure of the coronary arteries (Chen and Schäfer, 2009). On the other hand, tomographic reconstruction methods aim to reconstruct the 3D/4D volume of attenuation coefficients (Schoonenberg et al., 2009a). Specifically, we distinguish between the tomographic reconstruction of high contrast arteries from rotational coronary angiography and low contrast cardiac reconstruction from C-arm cone-beam CT (CBCT). In this review, we merely focus on the papers about high contrast coronary artery reconstruction.

The goal of this review is to identify the trends and the developments in the area rather than explaining application specific details. Moreover, we briefly aim to discuss the necessity of 3D/4D reconstruction and potential impact of those reconstructions on the clinical decision support systems and interventional planning. Compared with the previous reviews, we provide a more comprehensive technical overview of 3D/4D reconstruction from X-ray coronary angiography, focusing on the recent developments in the model-based and tomographic reconstruction. With respect to model-based reconstruction methods, we cover multi-view reconstruction techniques and put a special emphasis on 4D reconstruction and vascular lumen reconstruction. In addition, we discuss the progress in motion estimation and optimization techniques for tomographic reconstruction methods. We also discuss the methods on how to evaluate the performance of the reconstructions, and summarise available databases for validation and comparison purposes.

This review is organised as follows. Section 2 provides brief descriptions of the types of the C-arm based invasive X-ray coronary angiography systems. Section 3 justifies the necessity of 3D/4D reconstruction of coronary arterial trees from X-ray coronary angiography and discusses the potential uses in the diagnosis and the interventional guidance. Section 4 details the model-based approaches and tomographic reconstruction approaches to the 3D/4D reconstruction of coronary arteries from X-ray coronary angiography. A summary of these two sections are given in Tables 1–3. Section 5.1 discusses the methods of validation and comparison, and finally, Section 6 concludes the review.

2. Types of X-ray coronary angiography systems

Invasive X-ray coronary angiography is the visualization of coronary arteries using X-rays during catheter-based injection of iodine contrast material (Scanlon et al., 1999). X-ray coronary angiography essentially provides anatomical information about the coronary arteries and the morphology of the stenoses. It could also provide limited functional information such as blood flow in the main coronary vessels and the existence of collateral flow (Green et al., 2004).

Since X-ray coronary angiography creates 2D projection images of the complex 3D/4D anatomy of the coronary artery arteries, multiple images should be collected by placing X-ray source and detector in different positions to ease CAD assessment. Positioning is handled by C-Arm based angiography system (Fig. 1). C-arm is essentially a C-shaped device, which holds X-ray source and flat-panel detector (image intensifier in older systems). Depending on the setup, C-arm allows movement of X-ray source and the detector along several axes. In fact, the trajectory of the movement of C-arm is the fundamental design parameter that differs between different types of X-ray coronary angiography protocols.

Clinical decision making requires an appropriate number of angiography images which depends on the difficulty of the clinical case. On the other hand, several other factors should be taken into account for the design of an X-ray imaging protocol which may bound the total number of acquired angiography images: (i) Contrast material may cause chemotoxic adverse reactions (such as contrast-induced nephropathy) directly related to the dose, molecular structure, and physiochemical characteristics (Messenger and Casserly, 2009; McCullough, 2008). (ii) Modern X-ray coronary angiography systems equipped with automatic exposure control units that try to balance the image quality and the X-ray tube voltage parameters. Although automatic exposure control effectively limits the exposure to X-ray radiation, further reduction is desired for

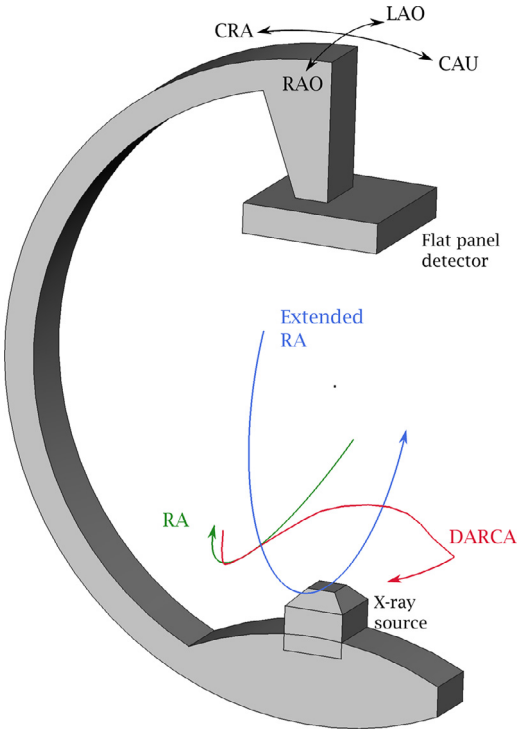

Fig. 1. C-arm trajectories for different X-ray angiography types: Typical trajectories that X-ray source follows during rotational X-ray angiography, extended rotational X-ray angiography, and DARCA are shown by green, blue, red curves, respectively.

increased safety. (iii) Finally, the procedural time is also another important matter due to the high number of percutaneous coronary interventions (PCI) (Go et al., 2014).

Standard X-ray angiography is the traditional way of X-ray coronary angiography, which consists of imaging the coronary arteries from a few fixed, operator chosen views. Therefore, the success rate of the diagnosis and the following treatment are solely dependent on the skills of the operator (Green et al., 2004). Although expert recommended views for standard X-ray angiography exist, they do not necessarily lead to satisfactory images due to the patient variability (Green et al., 2004). Even though standard X-ray angiography is currently the gold standard in interventional cardiology, it has some limitations in terms of contrast material use, procedural time and radiation exposure.

A biplane X-ray angiography system consists of two C-arms, which are generally configured to collect angiography images from orthogonal views. As a result, the biplane X-ray angiography system doubles the number of images that are acquired during a single contrast injection. However, operator dependency of the image acquisition quality persists.

Rotational X-ray angiography is an advanced scanning technique, which is devised to standardise and automatise the image acquisition (Green et al., 2004). It provides an operator independent, panoramic view of the coronary arteries by collecting a series of images during a predefined C-arm rotation (Tommasini et al., 1998). The continuity in the collected images help the operator to mentally visualise the dynamic spatial structure of the coronary arterial tree.

Traditionally in rotational X-ray angiography, rotation of gantry starts from 55° to 60° right anterior oblique (RAO) and ends at 55° to 60° left anterior oblique (LAO) with some cranial (CRA) or caudal (CAU) angulation. Extended rotational X-ray angiography is a novel acquisition protocol in which the arc that goes from 120° LAO to 60° RAO with no angulation is introduced (Fig. 1) (Klein et al., 2011). Extended rotational X-ray angiography facilitates the use of tomographic reconstruction based algorithms to reconstruct the contrast filled high contrast coronary arteries. However, it should be noted that extended rotational X-ray angiography is different than cardiac C-arm CBCT, which also provides tomographic reconstruction. Extended rotational X-ray angiography runs faster than cardiac C-arm CBCT and requires fewer images because it is used to reconstruct high contrast objects (Unzué Vallejo et al., 2013). Nonetheless, extended rotational X-ray angiography capability is also integrated into the state-of-the-art C-arm CBCT devices. Extended rotational X-ray angiography has some specific issues because of the prolonged acquisition time, such as prolonged contrast injection (Klein et al., 2011) and motion due to breathing.

Dual-axis rotational coronary angiography (DARCA) is an improved form of rotational X-ray angiography, which further increases the patient safety and eases the acquisition of the angiography images. DARCA combines the acquisitions with CRA and CAU angulation into one single acquisition run (Klein and Garcia, 2009). Moreover, the trajectories for the rotation of C-arm is not randomly selected but optimised in DARCA (Fig. 1). The optimised trajectories allows to collect images with minimal vessel overlap and foreshortening and consistent with the expert recommended views (Garcia et al., 2009).

3. Necessity and potential uses of coronary artery reconstruction

Despite the advent of 3D non-invasive imaging modalities (CCTA, MRA) to visualise the coronary arteries, 2D invasive X-ray coronary angiography is still considered the gold standard for the clinical decision making and therapy guidance due to several reasons (Mark et al., 2010). The technology is widespread and trained staff is available. Moreover, X-ray coronary angiography still delivers highest spatial and temporal resolution. More importantly, it is an interventional imaging modality, which does not only provide diagnostic information but also guides the following therapeutic procedures (Chen and Schäfer, 2009). However, X-ray coronary angiography is fundamentally limited since it could only produce 2D projection images of complex 3D anatomies of the coronary arteries. A 3D/4D reconstruction could (i) ease diagnostic decision making, (ii) assist pre-operative planning, (iii) provide intra-operative guidance, and (iv) supply virtual physiological indices.

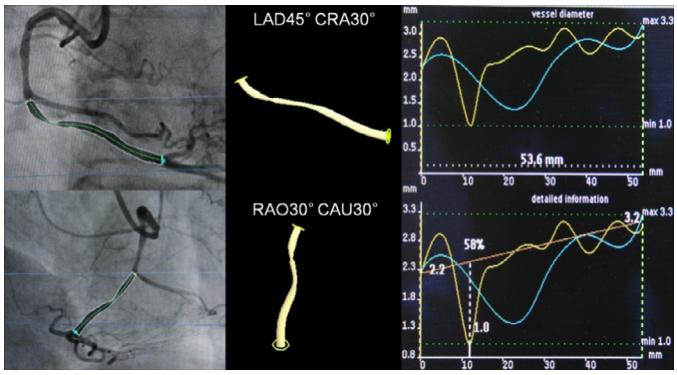

Fig. 2. Three-dimensional quantitative coronary angiography: Segment of interest is reconstructed from X-ray coronary angiography to obtain lesion measurements (e.g. vessel diameter along segment). Reprinted from Lee et al. (2012) with permission from authors.

Traditionally, the assessment of stenoses, the selection of the correct treatment for the patient, and the delivery of the treatment depend on operator's interpretation of 2D projection images (Chen and Schäfer, 2009). Lesion lengths, angles of bifurcations and vessel tortuosity may be misinterpreted in 2D projection images. In addition, subjective interpretation of 2D images could also lead to interobserver and intraobserver variability. More importantly, misinterpretation could also lead to over/under estimation of lesion severity and incorrect selection of stent size (Gollapudi et al., 2007; Eng et al., 2013). Consequently, suboptimal selection of the stent dimensions could reduce the effectiveness due to poor lesion coverage (Gollapudi et al., 2007), cause restenosis (Mauri et al., 2005) or thrombosis (Mauri et al., 2005; Moreno et al., 2005) and increase the cost of the treatment (Gollapudi et al., 2007). In order to overcome these diagnostic problems and select an optimal stent dimension, computerised measurements of lesions (such as minimum luminal area, percentage area stenosis, minimum luminal diameter etc.), which are considered to be correlated with the degree of the stenosis, are utilised (Pantos et al., 2009). This procedure is generally known as quantitative coronary angiography (QCA). With the development of 3D coronary artery reconstruction algorithms, QCA can now performed in 3D reconstruction of the lesion of interest (Fig. 2) (Dvir et al., 2008; Garcia et al., 2007), which is shown to be in an agreement with ground truth measurements via guidewire or IVUS measurements (Agostoni et al., 2008; Lee et al., 2012; Meerkin et al., 2010; Neubauer et al., 2010).

Image fusion is another emerging field in medical imaging. It aims to supply complementary information (anatomical/functional information, pre/post-operative information, device visibility, soft tissue visibility) from different imaging modalities. Specifically, X-ray coronary angiography could be supplemented by pre-operative 3D images from CCTA, cross-sectional morphology information from IVUS or OCT. Fusion of X-ray coronary angiography with pre-operative CCTA could bring the intervention planning visually into the cath-lab (Rivest-Hénault et al., 2012) and provide additional information especially in the patients with chronic total

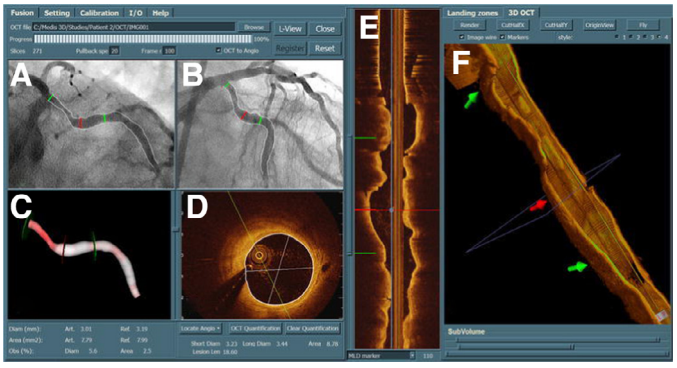

Fig. 3. Fusion of X-ray coronary angiography with OCT: Corresponding locations are shown with the same colors in different views. Fusion provides clinician with complementary information from both modalities for the assessment of vessel lumen. Reprinted from Tu et al. (2012) with permission from authors.

occlusions (Baka et al., 2013; Dibildox et al., 2014). Although most of CCTA/X-ray coronary angiography fusion algorithms are formulated as 2D/3D registration (Rivest-Hénault et al., 2012; Baka et al., 2013), one recent study showed that the problem can be cast as a 3D/3D registration problem by the help of 3D reconstructions from biplane X-ray angiography (Dibildox et al., 2014). Fusion of X-ray coronary angiography with IVUS or OCT is also desirable since these imaging modalities are known to provide cross-sectional morphological information about the stenosis and plaque characteristics (Bruining et al., 2009). This type of fusion employs 3D reconstruction of coronary artery centreline and complements it with the surface information from IVUS/OCT (Fig. 3) (Bruining et al., 2009; Tu et al., 2012).

The search for the link between the coronary anatomy and its physiology has led to a remarkable amount of research carried out in the image based hemodynamics modelling field (Taylor and Steinman, 2010; Zhang et al., 2014). Large scale randomised clinical studies reveal that significance of a coronary stenosis could not be determined solely on anatomical information and conclude that anatomical information from any imaging modality should be coupled by intra-coronary physiological measurements (Kern et al., 2006). Among those physiological measurements, a comprehensive investigation is devoted to fractional flow reserve (FFR) (Pijls et al., 2007; Tonino et al., 2009). Recently, there is a strong interest in estimating virtual FFR values using the flow and pressure values obtained through CFD simulations inside 3D anatomical models of the coronary arteries (Johnson et al., 2013; Morris et al., 2015). Virtual FFR via non-invasive imaging (CCTA, MRA) could pave the way for a non-invasive diagnosis of moderate stenosis. On the other hand, it is also feasible to calculate virtual FFR from the 3D reconstruction obtained from invasive X-ray coronary angiography (Morris et al., 2013; Papafaklis et al., 2014; Tu et al., 2014).

Although there is a plethora of research evidence that highlights the clinical potential of the aforementioned applications, a large amount of the research carried out over the last ten years is still not ready for prime time and is unfortunately not available in clinical routine. There are, however, a number of methods that start appearing as part of clinical research (see, for instance (Campbell and Mahmud, 2014; Ligthart et al., 2014; Morris et al., 2013; Tu et al., 2014; Calmac et al., 2015; Lansky and Pietras, 2014)). One of the major limiting factors for their translation into the clinics is that 3D reconstruction still needs to be simultaneously robust, accurate and real-time and meeting these three constraints at once has proven really challenging. As method become more involved to deal with accuracy, they tend to be computationally expensive and sensitive to various parameters. As techniques attempt to achieve speed, they become prone to inaccuracies and lack robustness. To date, most of the commercially available algorithms still rely on intensive off-line manual interactions. Over the last few years, while parallel efforts on addressing this requirement trilogy has continued, many researchers have also focused on extracting functional or physiological information from imaging in addition to anatomical information (Lansky and Pietras, 2014). However, automated algorithms that could provide reconstructions in (near) real-time are still required as input to these methods so the quest for accurate, robust and efficient algorithms for coronary anatomy reconstruction continues.

4. Reconstruction of coronary arteries from X-ray coronary angiography

In recent years, a significant amount of work has been devoted to obtain a 3D/4D representation of the coronary tree from X-ray coronary angiography. Different types of X-ray coronary angiography systems, strategies to handle cardiac and respiratory motion, and additional requirements have resulted in the diversity of the coronary artery reconstruction methods. Nevertheless, the methods in the literature could be classified into two main groups, namely model-based reconstruction (modelling) (Section 4.2) and tomographic reconstruction (Section 4.3). The main distinction between two classes of reconstruction methods is the reconstruction output. While modelling generates a binary 3D/4D representation of the coronary arteries, tomographic reconstruction produces a volume representing the X-ray absorption of the coronary arteries. Despite the separation of reconstruction methods, there are some general aspects, which are applicable to both classes. These aspects are discussed in Section 4.1.

4.1. General aspects of the reconstruction methods

4.1.1. X-ray coronary angiography type

One fundamental aspect is the selection of X-ray coronary angiography type. Due to specific requirements of the reconstruction methods, all types of X-ray coronary angiography are not suitable for both types of reconstruction (Section 2). While all types of X-ray coronary angiography are suitable for modelling, only rotational X-ray angiography allows tomographic reconstruction.

4.1.2. Image acquisition geometry and calibration

Another common aspect is the acquisition geometry. The acquisition geometry for reconstruction methods is commonly described using the tools from the computer vision, since the acquisition principle of X-ray is similar to the finite projective camera model (Hartley and Zisserman, 2004)[1]. The main difference is that the X-ray images are magnified. Three coordinate systems are defined for the acquisition geometry, namely, X-ray source (camera), X-ray detector (image) and patient coordinate systems (Fig. 4). X-ray source coordinates are centred at X-ray source location (camera centre). Flat panel X-ray detector is modeled with a plane (image plane) perpendicular to one of the main axis of the X-ray source coordinate system. Distance between the X-ray source and X-ray detector is known as source to image distance (SID). The line from the X-ray source perpendicular to X-ray detector is known as principal line and it intersects X-ray detector at principal point. Image formation is determined by intrinsic parameters of the camera model, which are SID, coordinates of the principal point in the X-ray detector coordinate system, and sometimes skew parameter. These parameters form a matrix called camera calibration matrix,

[1] This is a simplification of the system model. Non-standard scan geometries can be incorporated using iterative tomographic reconstruction methods (see Section 4.3.1).

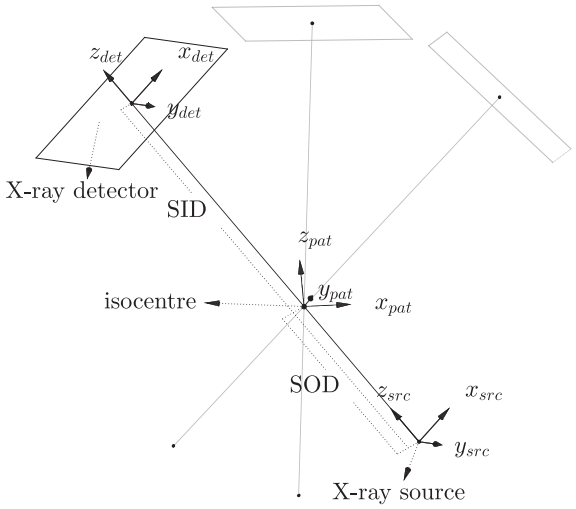

Fig. 4. X-ray coronary angiography image acquisition geometry: Three coordinate systems, which are related to each other by a rigid transformation, are defined for X-ray detector, patient, and X-ray source. The origin of the patient coordinate system is typically assumed to coincide with the isocentre (centre of rotation of the gantry). Intrinsic and extrinsic parameters specify the mapping between patient and detector coordinates.

which is used to describe the mapping between points given in X-ray source coordinates and their 2D projection given in 2D X-ray detector coordinates. The centre of rotation of the gantry is called isocentre and considered to be the origin of the patient coordinate system. It is generally assumed to lie on the principal line. The relation between the X-ray source and patient coordinates is described by a rigid transformation. The parameters (rotation angles and source to object/patient distance (SOD)) for the rigid transformation are known as extrinsic parameters. Intrinsic and extrinsic parameters constitute camera projection matrix, which defines the mapping between patient and X-ray detector coordinate system[2]. The acquisition geometry enables us to define another important concept called projection line. A projection line for a point is the line that passes through the X-ray source and the projection of the point in the X-ray detector.

One minor point is the image distortion related to the X-ray detector. Older angiography systems are equipped with image intensifier that generates images with distortion due to its design. These distortions must be corrected either before applying the reconstruction method (Shechter et al., 2003a) or within the reconstruction method (Cañero et al., 2000). However, now the new angiography systems make use of flat panel detectors, which can create distortion free X-ray images (Strobel et al., 2009).

It is necessary for both class of reconstruction methods to obtain the parameters describing the acquisition geometry. However, the way how the acquisition geometry obtained changes between different reconstruction strategies. Some methods rely on a prior calibration step to record the geometry parameters. During the image acquisition the X-ray gantry follows the recorded geometry to generate the X-ray coronary angiography images. In earlier, mechanically unstable C-arm systems, calibrations can be performed just before image acquisition (Wiesent et al., 2000). However, in stable C-arm systems, the calibration is performed once in a while with regular intervals to ensure its stability (Rougée et al., 1994; Koppe et al., 1995; Fahrig et al., 1997). The calibration is usually completed by using phantom objects (Wiesent et al., 2000; Rougée et al., 1994; Koppe et al., 1995; Fahrig et al., 1997). Nevertheless, some methods opt for non-calibrated data because of the possible table translation during image acquisition or because of noise in the calibrated parameters. These methods either estimate geometry parameters before computing the reconstruction or jointly estimates the geometry parameters and the reconstruction. However, joint optimization aggravates the problem by increasing the ill-posedness of it, and is not really realistic. On the other hand, all of the tomographic coronary artery reconstruction methods assume calibrated geometry, while modelling based reconstruction can adopt calibrated and non-calibrated geometries (Section 4.2).

[2] Modern X-ray imaging systems store both extrinsic and intrinsic parameters.

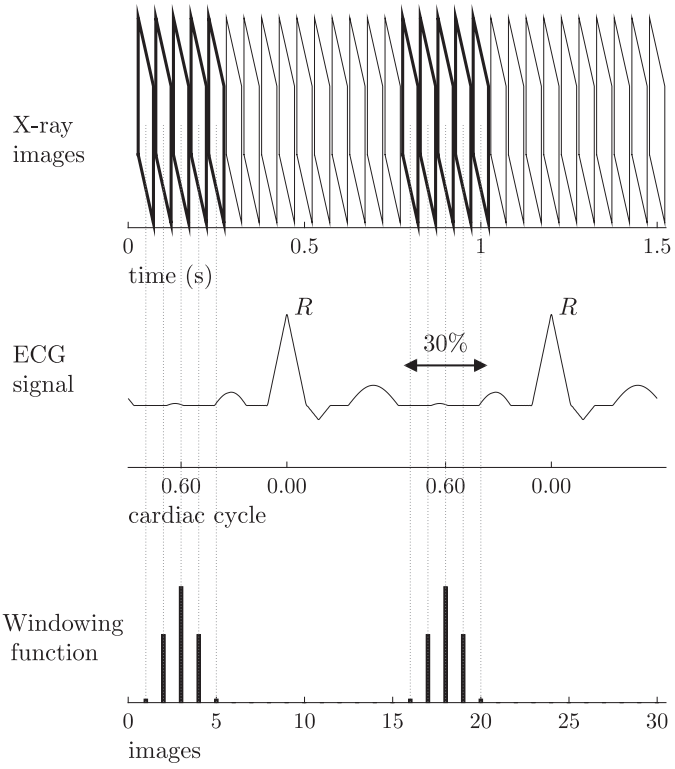

Fig. 5. Retrospective ECG gating: A subset of images corresponding to the same cardiac phase are selected to discard the cardiac motion before reconstruction (top). Each image is assigned a cardiac phase using the ECG signal recorded simultaneously with the image acquisition (middle). A windowing function specifies a temporal slot and weighting for image selection (bottom).

4.1.3. Handling of cardiac and respiratory motion

Another important aspect with regard to both classes of reconstruction is the respiratory and cardiac motion experienced by coronary arteries during image acquisition. Respiratory motion could be reduced during the acquisition by asking the patients to hold their breaths (see Tables 1 and 2). Considering there is no residual respiratory motion, retrospective gating strategies are commonly utilised to overcome cardiac motion. The main principle of retrospective gating is to select the subset of images that are at the same cardiac phase in order to eliminate the cardiac motion. The number of available cardiac cycles during the acquisition is important; high heart rates are preferable to low or normal cardiac phase in order to have sufficient number of images for reconstruction. Two different approaches are investigated for retrospective gating: ECG and surrogate based gating.

The most common way to achieve gating is to use ECG signal simultaneously acquired with the image acquisition. Specifically, this signal is used to assign cardiac phases to the collected X-ray images assuming a cyclic heart motion (Fig. 5). Typically, the phases of least motion, end-systole and end-diastole (Shechter et al., 2006; Husmann et al., 2007), are employed for gating to obtain a higher 3D reconstruction quality.

Missing or unusable ECG (e.g. due to mislocation of electrodes), and irregular heartbeats pose further challenges for retrospective gating of images collected using a C-Arm system (Rohkohl et al., 2008b, 2009b). In X-ray coronary angiography, motion phases can be assigned based on a surrogate function extracted from the intensity information in the X-ray images (Blondel et al., 2006; Lehmann et al., 2006). To find such a surrogate function, several assumptions are made. First, it is assumed that there is no CRA/CAU angulation during acquisition and consequently axial direction of the patient is roughly aligned with vertical axis of the X-ray detector. Second, predominant motion in the axial direction is assumed to be caused by the cardiac motion. Under these assumptions, motion in the axial direction can be used as the surrogate function. Blondel et al., 2006 determined the motion by estimating the shift between horizontal line integrals of subsequent X-ray images. Lehmann et al., 2006 calculated centroid of the horizontal line integrals and use its motion to define the surrogate. From a different perspective, these methods find an optimal time point to compute the reconstruction.

A related problem is to select the optimal cardiac phase for the reconstruction, given the gating signal. Because of the heart rate differences and other special conditions (e.g. arrhythmia) of the patients, the optimal cardiac phase for reconstruction is different between the patients (Husmann et al., 2007). Moreover, it is known that the reconstruction quality varies among different cardiac phases (Schäfer et al., 2006). Apart from using aforementioned surrogate functions, several methods are devised to determine the optimal phase. The methods described in Rasche et al. (2004, 2006a) build a series of gated reconstructions and define a quality metric based on the histogram analysis of those reconstructions. The mean intensity value of the high contrast voxels are used as the quality metric. Hansis et al. (2008b) used minimum intensity projections of a back-projected distance map to determine a quality measure for the cardiac phases assigned via ECG signal.

The selection of images are generally conducted by a windowing function. A windowing function defines a temporal slot around the selected cardiac phase; the X-ray images inside that domain are selected for reconstruction. The shape of the windowing function introduces a weighting to X-ray images depending on temporal distance of X-ray image to the selected phase. Most commonly used windowing functions are nearest-neighbour (Schäfer et al., 2006; Rasche et al., 2006b) or power of cosine function (Schäfer et al., 2006; Rohkohl et al., 2008a; Schwemmer et al., 2013b). The nearest-neighbour function selects the image that is closest to the selected cardiac phase. This gating function strictly eliminates the cardiac motion by selecting one image for each cardiac cycle. However, it severely undersamples available X-ray projection data and this can lead to artifacts in the reconstruction (Schäfer et al., 2006). Instead of nearest-neighbour gating, bell-shaped functions are also used as the windowing function. One popular choice is cosine squared windowing function (Schäfer et al., 2006). A more general family of cosine functions, namely power of cosines, are introduced in Rohkohl et al., 2008a. Specifically, the shape of the windowing function is controlled using a parameter describing the power of the cosine function. In addition, there are also some attempts to determine the optimal window length from X-ray images using value of the surrogate function (Lehmann et al., 2006). Finally, one should note that cardiac motion type (e.g. twisting motion (Unberath et al., 2015)) and magnitude could still lead to undersampling problems even using bell-shaped or surrogate based windowing functions.

4.2. Model-based reconstruction

Model-based reconstruction (or modelling) methods try to build a 3D/4D binary model of coronary arteries, which consists of a 3D/4D centreline and, occasionally, the vessel surface. These methods are flexible tools for reconstruction, since they allow us to use images from all X-ray coronary angiography modalities or from calibrated and non-calibrated systems. However, the flexibility is usually accompanied by requirement of manual processing. Although these methods commonly use ECG gating to remove the motion of coronary arteries (Table 1), there are efficient ways to propagate the 3D reconstruction for one cardiac phase to the remaining phases to obtain 4D reconstruction.

Based on the overall design, modelling methods could be further divided into two groups, namely forward-projection based (Section 4.2.1) and back-projection based (Section 4.2.2) methods. Modelling methods could also differ in terms of ability to obtain 4D reconstruction (Section 4.2.3), multi-view modelling capability (Section 4.2.4) and vascular lumen reconstruction (Section 4.2.5).

4.2.1. Forward-projection based methods

Forward-projection based modelling methods for coronary artery reconstruction employ a 3D model, which adapts itself to the vessel structures in 2D X-ray projection images.

Deformable models are frequently employed in forward-projection based reconstruction. The deformable model evolves under the influence of an external energy, which is obtained from the 2D images and an internal energy, which is due to the smoothness and topology of the model itself. The most commonly used 3D deformable model for modelling of the coronary arteries are active contour model (Kass et al., 1988). In the context of coronary reconstruction, each coronary artery branch is represented by one active contour model and these models are optimised individually. The main concern for active contour based reconstruction is the design of the external and internal energy terms.

Two-dimensional external energy terms are generally computed using the image information from the 2D projection images and used in various ways to update the location of the 3D landmark points describing the active contour. In order to calculate 2D external energy terms for each landmark point, common approaches are to compute the Gradient Vector Flow (GVF) (Xu and Prince, 1998b), Generalized Gradient Vector Flow (GGVF) (Xu and Prince, 1998a), and Potential Energy (PE) (Cohen and Cohen, 1993) from the 2D projection images and use the resulting 2D vector fields (Cañero et al., 2000, 2002; Cong et al., 2013, 2015; Yang et al., 2014). Centrelines segmented from 2D projection images are used as the feature map input to GVF, GGVF and PE computation. Alternative to this approach, image intensity information can be directly used to compute the external energy term. The intensity values are locally minimum at the image pixels corresponding to the vessel axis, since X-rays passing through the vessel axis penetrate the thickest layer of contrast (Hui and Friedman, 2002). The direct (Hui and Friedman, 2002) or normalised (Zheng et al., 2010) sum of intensity values from different projection images are used to formulate the external energy term. In Zheng et al., 2010, authors also added the gradient of the intensity to the formulation to gain some robustness to noise on the 2D pixel values.

In order to update the position of the 3D landmark points of the active contour, one strategy is to update the projections of the landmark in 2D (Cañero et al., 2000, 2002). Specifically, the 3D landmarks for the current iteration of the active contour evolution are projected onto the 2D images. The 2D projections of landmarks are moved to new locations in 2D according to the external force. Because of the epipolar geometry, a new 3D position for the landmark must located at the intersection of the projection lines. However, updated 2D projections do not comply with the epipolar constraints, since they have been updated independently in the projection images. Therefore, the new 3D position of the landmark is found as the 3D position, which minimises the distance to all projection lines (Fig. 6a). Another strategy is to compose a 3D

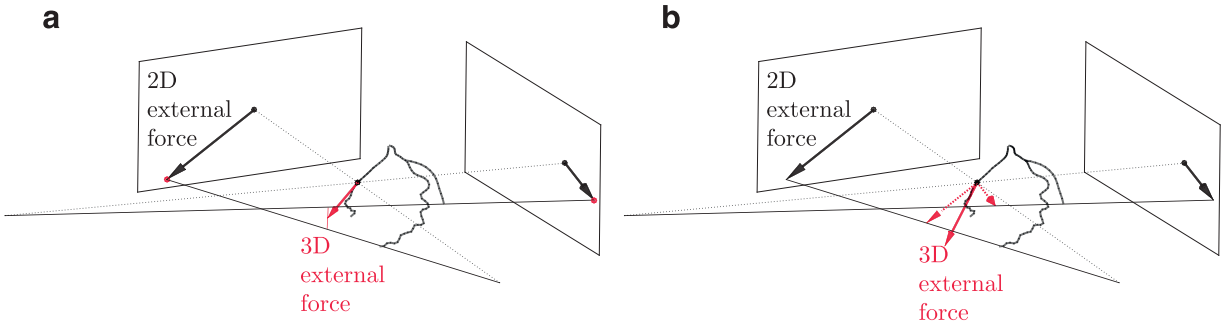

Fig. 6. Computation of external force for active contour based reconstruction methods: (a) 3D external force can be computed using new 2D locations updated using 2D external forces. (b) Alternatively, 3D external force can be computed using back-projections of the 2D external forces.

external force term using the 2D external force terms (Cong et al., 2013, 2015; Yang et al., 2014). To this end, the 2D external forces are back-projected onto the patient coordinate system by ignoring the out-of-plane component of the 3D external force. The back-projected external energy forces are added together to obtain the 3D external force (Fig. 6b). The main advantage of this strategy is to update the 3D landmark points without violating the epipolar constraints, which is proven to increase the accuracy and the convergence rate (Cong et al., 2015; Yang et al., 2014). Additionally, this strategy is easy to adapt to multi-view scenarios since the 3D external force is given by a simple vector addition operation (Cong et al., 2015).

As the internal energy, the elastic and bending energy from the original active contour model (Kass et al., 1988) are generally used. (Zheng et al., 2010) devised a new elastic term to avoid shrinkage problem of the open active contour model. This new term produces an additional penalty for the landmark pairs, which are not separated by the average distance between all pairs of neighbouring landmarks.

Initialization of the active contour model in 3D is performed manually (Cañero et al., 2000, 2002; Cong et al., 2013, 2015; Yang et al., 2014; Hui and Friedman, 2002; Zheng et al., 2010). Some corresponding points (including the start and end point) for a branch are selected from different views and rough reconstructions are obtained for these points. These points are used to generate a piecewise linear active contour model to start with.

Although the literature on the forward-projection based modelling of coronary arteries revolves around parametric active contour models, there are some exceptions to this trend. As one notable example, (Sarry and Boire, 2001) used Fourier descriptors as the parametric deformable model. An analytical relationship between the 3D Fourier descriptor and its projection is derived. This relationship yields to an energy functional, which consists of intensity, epipolar constraint and smoothness terms. Another interesting example uses geometric active contours as the deformable model (Keil et al., 2009). A 3D level set surface for the coronary artery is defined in a reference cardiac phase. It is assumed that this level set surface is mapped to a 2D projection image by rigid transform due to motion of the arteries followed by a projection operation. An energy minimization framework is formulated to evolve the level set in the reference phase and to estimate the rigid transformation for all the projection images. Çimen et al. (2014) used a statistical bilinear model of ventricular epicardium as spatio-temporal model, and estimated parameters of the bilinear model along with the arterial locations on the bilinear model.

Forward-projection based modelling methods do not require any correspondence between centrelines extracted from 2D X-ray images. Moreover, 2D segmentations are unnecessary for some of the methods, which work directly on the intensity values. These features provide serious advantages over most of back-projection based modelling methods in the literature. In addition to that, it is easy to adapt forward-projection modelling methods for reconstruction from multiple views. However, these methods rely on manual selection of corresponding points from projection images for each branch of the artery, which might be time consuming and prone to errors.

4.2.2. Back-projection based methods

Back-projection based modelling methods build the coronary artery tree from back-projection of 2D information extracted from projection images that are selected via ECG gating. These methods could be divided into two main groups: (i) methods based on 2D feature matching, and (ii) methods based on back-projection of vesselness responses.

The first group of back-projection based methods are the methods based on 2D feature matching. These methods start with a segmentation of artery centrelines and often several salient structures (e.g. start/end points, bifurcations) from the projection images. Correspondences are established between the centrelines from different views using epipolar geometry, and 3D points representing the coronary artery tree are reconstructed using the triangulation method (Hartley and Zisserman, 2004) from the computer vision (Fig. 7a).

Two-dimensional feature matching based modelling methods are designed to work with the non-calibrated systems (Hoffmann et al., 2000; Chen and Carroll, 2000, 2003; Mourgues et al., 2001; Blondel et al., 2006; Fallavollita and Cheriet, 2008; Yang et al., 2009), although exceptions exist (Cardenes et al., 2012; Movassaghi et al., 2004). This is because the estimation of geometry parameters that relate the projection images used for reconstruction can be easily integrated into the method. One way is to estimate the geometry parameters before reconstruction commences. For this purpose, the salient points (e.g. start/end, flexion and bifurcation points) that are extracted during the segmentation step are exploited (Hoffmann et al., 2000; Chen and Carroll, 2000, 2003; Andriotis et al., 2008). A set of corresponding points are formed via manual establishment of correspondence. This set can be used to write constraint equations using the fundamental or essential matrix (Hoffmann et al., 2000) or to formulate an energy function whose minimum is given by the optimal values for the geometry parameters (Chen and Carroll, 2000; 2003). Generally, rotation and translation between the X-ray sources are considered to be the geometry parameters to optimise, and intrinsic parameters are assumed to be known. The energy function mainly consists of the reprojection error of points and the reprojection error of direction vectors (Chen and Carroll, 2000, 2003; Andriotis et al., 2008). Another popular way is to estimate geometry parameters jointly with the reconstruction. In this strategy, estimation of the geometry parameters and reconstruction, and the establishment of the correspondences are iteratively performed until a convergence criteria is met (Mourgues et al., 2001; Blondel et al., 2006; Fallavollita and Cheriet, 2008; Yang et al., 2009). These methods are advantageous

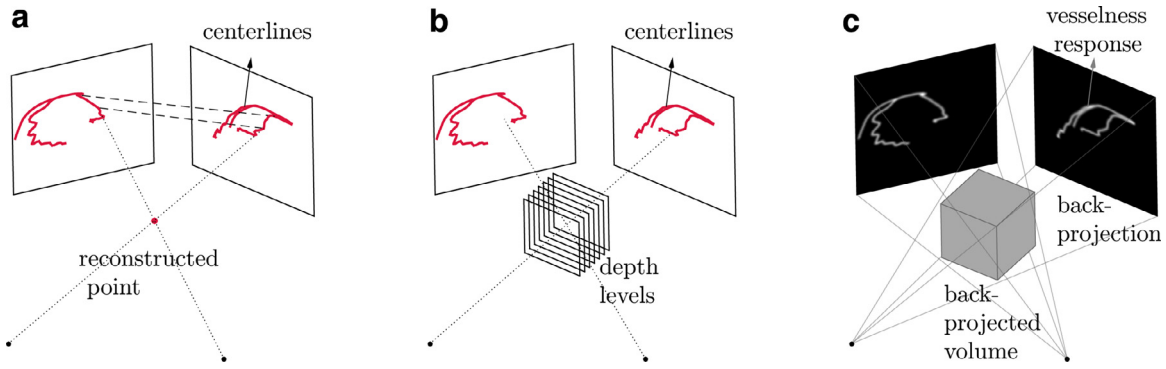

Fig. 7. Summary of back-projection based methods: (a) Methods based on 2D feature matching establish correspondences of centrelines from different 2D views and compute reconstruction using triangulation. (b) Some of the 2D feature matching based methods divide the 3D space into parallel planes representing the depth levels. Each centreline point in the reference frame is assigned to one of the depth levels using the information from multiple X-ray images. (c) Methods based on back-projection of vesselness response compute a 3D volumetric vesselness response from 2D vesselness responses for further processing.

because they are robust against outliers and provide a mechanism to estimate the intrinsic parameters as well. In Yang et al. (2009) a total of 14 parameters are optimised including intrinsic (SID, principal point coordinates, skew) and extrinsic parameters (rotation, translation, table translation). For any approach to estimate the geometry parameters, initialization is important. In most of the cases, the geometry parameter estimation starts from the values recorded by the X-ray system.

Correspondence establishment is the critical step for feature matching based methods, since the corresponding points are directly used to triangulate the 3D position. The simplistic approach is to use hard epipolar constraints to establish the correspondences (Hoffmann et al., 2000; Chen and Carroll, 2000, 2003; Andriotis et al., 2008). However, epipolar lines usually do not produce a single match and this necessitates more sophisticated approaches. One solution is the exploitation of dynamic programming algorithms. Yang et al. (2009) used a method similar to dynamic time warping (DTW) (Sakoe and Chiba, 1978) to find the correspondences. Dynamic programming can also be used to put soft epipolar constraints (Mourgues et al., 2001; Blondel et al., 2006). Soft epipolar constraints allow for a point in the first view to match a point in the second view that is not strictly on the epipolar line but around it. To this end, an energy function is formulated for matching that consists of unary and binary terms. Unary terms penalise according to the distance to the epipolar line (Mourgues et al., 2001) or any feature that reflects correct correspondence (e.g. high tubularity value) (Blondel et al., 2006). On the other hand, binary terms ensure that the linked points in the first view are paired with points that are close to each other in the second view (Blondel et al., 2006) or ensures that the deviation from epipolar lines varies smoothly (Mourgues et al., 2001). In order to avoid point-to-point correspondences, a branch-to-branch correspondence establishment method is proposed in (Cardenes et al., 2012). The projection lines formed by the 2D points in the projection images and corresponding X-ray source position form ray bundles for each view. Closest points on the ray bundle from first view with respect to the ray bundle from the second view establishes a correspondence. Another way to support the correspondence finding is to estimate some 3D features from 2D features and use the estimations to put a constraint on the correspondences. One particular example is the study in Fallavollita and Cheriet (2008). Given an initial correspondence, 3D curvature value for a point is estimated from the 2D curvature values from projection images. They compared estimated curvature and the curvature obtained from the reconstruction for the initial correspondence, and if the values are very different from each other the point correspondence is discarded. Although the authors used it for outlier removal, it is a promising strategy to put prior information on the 3D reconstruction.

One alternative strategy for 2D correspondence establishment is proposed in Liao et al. (2010) and later adapted for dynamic reconstruction in Liu et al. (2014b). The problem is formulated as a depth map estimation, inspired by multi-view stereo in the computer vision literature. To this end, the 3D space between X-ray source and detector is divided into parallel planes of equal depth increments (Fig. 7b). To obtain the reconstruction, all 2D centreline points in one reference view are assigned to a plane, i.e. assigned a depth value using an energy function minimization. Liao et al. (2010) proposed an energy function consisting of a reprojection error term and a term for smoothness of depths in 3D. The energy minimization can be performed through efficient methods such as graph cuts or belief propagation (Szeliski et al., 2008).

Modelling methods based on 2D feature matching provide flexible and modular approaches to reconstruction. There is a wide selection of methods to choose from for segmentation, estimation of imaging geometry, and establishing the correspondences. More importantly, their ability to estimate the imaging geometry is indispensable for reconstruction from standard X-ray angiography, since table movements are common during image acquisition. Requirement of 2D segmentation is the main disadvantage of these methods. First, it hinders its use for multi-view reconstruction because segmentation of 2D projection images is generally a demanding (especially if there is overlap and foreshortening) and time consuming task. Second, one should select projection images at the same cardiac phase, with some angular difference (between 35–145 degrees (Movassaghi et al., 2004)), without overlap and foreshortening, and with sufficient contrast. These conditions may not be satisfied easily and as a result the method may output suboptimal reconstructions.

The second group of back-projection based methods are the methods based on back-projection of vesselness responses. These methods compute vessel responses, which highlight coronary arteries in 2D projection images. These responses are back-projected given the imaging geometry to compute a volumetric vessel response in 3D. Segmentation methods are applied on the 3D vessel response to obtain the coronary artery reconstruction (Fig. 7c).

The first choice for these methods is the type of the 2D vessel response. Binary segmentation (Law and Chan, 2003), tubularity response (Jandt et al., 2009a), and distance map to centreline (Li and Cohen, 2011) are used in the literature. Second choice is the back-projection operator. Different operators have been studied in the literature, namely multiplicative combination from all views (Law and Chan, 2003), weighted multiplicative combination from all pairs of views (Jandt et al., 2009a) and maximum of 2D

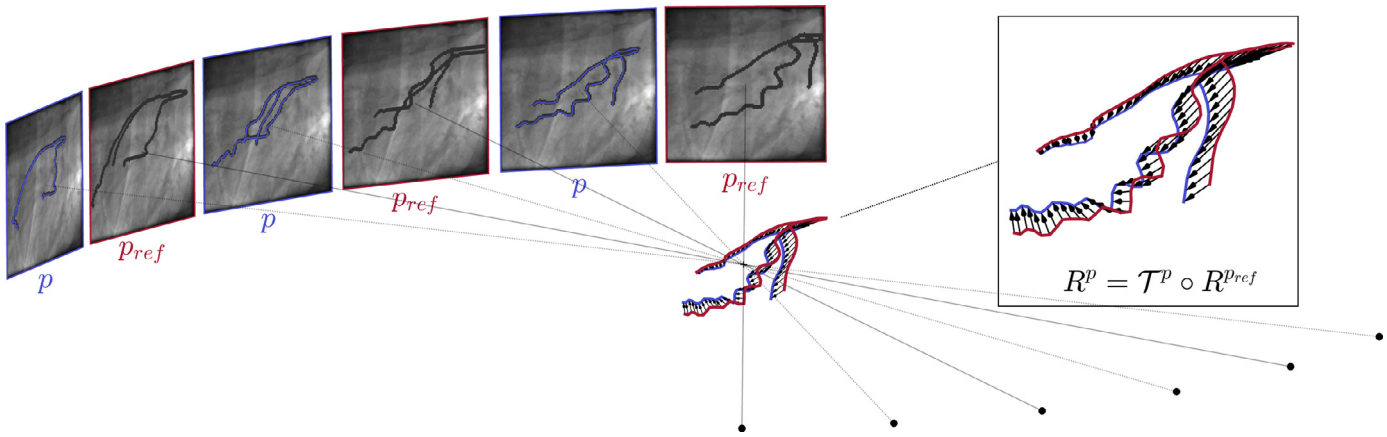

Fig. 8. Propagation of initial 3D reconstruction by transformation optimization: The transformation for cardiac phase p (T^p) is estimated such that the projection of deformed initial reconstruction is aligned with the vessel structures in 2D projection images at phase p. The initial reconstruction (R^{ref}) at the reference phase p^{ref} and deformed initial reconstruction (R^p) at phase p are shown in red and blue, respectively.

distances to centrelines (Li and Cohen, 2011). Three-dimensional segmentations can be obtained from a variety of methods, although fast marching propagation (Law and Chan, 2003; Jandt et al., 2009a) and minimal paths (Li and Cohen, 2011) are the only ones used so far. Owing to low number of projection images, 3D vessel responses are generally very noisy and robust methods for segmentations are required. Otherwise, post-processing steps might be required to prune the segmentation (Law and Chan, 2003; Jandt et al., 2009a).

Modeling methods based on back-projection of vesselness response work with minimum level of interaction. Additionally, being inherently multi-view is a merit, however these methods might require extended rotational X-ray angiography images to increase the number of images available for reconstruction and to reduce the noise in the 3D vessel response function.

4.2.3. 3D+time (4D) model-based reconstruction

3D+time (4D) reconstruction of coronary arterial tree could give the clinician a better assessment of the target lesion by providing information about motion and extent of deformation near the lesion (Chen and Carroll, 2003). Modeling methods could be extended such that they have the ability to generate 4D reconstructions of coronary arteries.

The most straightforward 4D reconstruction strategy to obtain 3D reconstructions for a number of cardiac phases separately (Chen and Carroll, 2003; Mourgues et al., 2001; Jandt et al., 2009b; Cardenes et al., 2012). This could be achieved by completely handling the reconstruction for each cardiac phase independent from each other (Chen and Carroll, 2003; Jandt et al., 2009b). To avoid complete independence of reconstruction at different cardiac phases, temporal constraints penalizing the difference between neighbouring cardiac phases can be used (Liu et al., 2014b). The disadvantage of processing each cardiac phase individually is the requirement of segmentations for every cardiac phase, which may sometimes be infeasible. Another drawback of working on each cardiac phase separately is that the resulting 3D reconstructions are independent from each other and there is no notion of temporal correspondence. If the motion field for the coronary artery tree is needed, temporal correspondences should be sought (Chen and Carroll, 2003; Jandt et al., 2009b). This can be achieved by branch matching or tree matching algorithms. For example, (Chen and Carroll, 2003) proposed a branch matching algorithm using a physics based principle to formulate matching energy. Jandt et al. (2009b) devised an energy formulation for iterative matching of tree structures.

A popular strategy for 4D reconstruction is to propagate an initial 3D reconstruction from a reference cardiac phase to the rest of the phases (Hui and Friedman, 2002; Zheng et al., 2010; Sarry and Boire, 2001; Shechter et al., 2003a; Bouattour et al., 2005; Tsin et al., 2009). Depending on the reconstruction methodology, there are two ways to accomplish this propagation. If it is a forward-projection based modelling method, the 3D deformable model representing the reconstruction for the reference cardiac phase is evolved such that its projection fits to the 2D projection images corresponding to the other cardiac phases. The easiest way is to use the 3D reconstruction as the initialization at the next cardiac phase and to apply the same reconstruction strategy (Sarry and Boire, 2001). However, this strategy does not introduce any temporal constraints. To overcome this drawback, the deformable model energy for 3D reconstruction might be enriched with some additional terms that enforce temporal smoothness (Hui and Friedman, 2002; Zheng et al., 2010). Four-dimensional propagation strategies for forward-projection based methods are generally designed to work with intensity values of 2D projection images in order to avoid the necessity of centreline segmentations for all the 2D images. On the other hand, back-projection based modelling method approaches 4D reconstruction as a temporal transformation estimation problem. Specifically, these methods parameterize a 3D/4D transformation, which is applied to the reference 3D reconstruction, such that the projections of the deformed reconstruction align with the 2D projection images (Fig. 8) (Shechter et al., 2003a; Bouattour et al., 2005; Tsin et al., 2009; Blondel et al., 2006; Bousse Ast et al., 2009). A rigid or affine transformation for each cardiac phase is optimised in Tsin et al. (2009). A set of hierarchical transformations with increasing degrees of freedom are proposed to model the motion of the arteries in Shechter et al. (2003a), Bouattour et al. (2005). Specifically, rigid, affine and 3D B-spline transformations are optimised respectively for each time step. A strategy to reduce the number of transformation parameters by estimating a transformation separately for each coronary artery branch is followed in Bouattour et al. (2005). A 4D B-spline transformation model is used in Bousse Ast et al. (2009). Instead of directly estimating the parameters of the transform, a motion vector field is calculated using an energy minimization. A second energy minimization is performed to estimate the parameters of the transformation using the motion vector field. In Blondel et al. (2006), temporal dimension is added to the transformation via a 4D B-spline transformation. To estimate the parameters of the transformation, an energy measure describing the quality of fit is used to estimate the parameters of the transformations. The

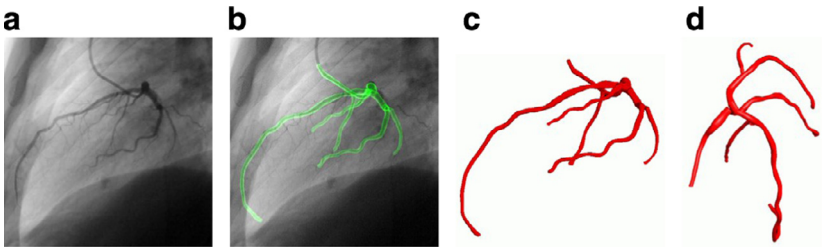

Fig. 9. An example of vessel lumen reconstruction: (a) X-ray image. (b) The forward projection of reconstructed vessel lumen onto the X-ray image. (c)–(d) Surface rendered views of reconstructed model in the left-right and cranio-caudal direction. Reprinted from Jandt et al. (2009b) with permission from IOP Publishing.

energy term consists of a term for the projection error, a term to constrain structural changes and a term to ensure smooth transformation. In order not to segment centrelines, the projection error term generally depend on intensity based features such as tubularity measure (Shechter et al., 2003a; Bouattour et al., 2005; Blondel et al., 2006) or GVF (Tsin et al., 2009). The energy term controlling the smoothness of deformation can be defined using the transformed points (Tsin et al., 2009) or using the parameters (e.g. control points for B-spline transformation) of the transformation (Shechter et al., 2003a; Bouattour et al., 2005; Blondel et al., 2006; Bousse Ast et al., 2009). Application specific temporal or structural constraints, such as cyclic deformation constraint (Tsin et al., 2009) or length preservation constraints (Shechter et al., 2003a), are taken advantage of as additional energy terms.

4.2.4. Multi-view model-based reconstruction

X-ray rotational X-ray angiography and DARCA offer a sequence of projection images from different views, which provides additional information for model-based reconstruction. Many state-of-the-art modeling methods benefit from the additional information. These methods differ in the way they use multiple projection images.

There are various ways to incorporate multiple views. Cong et al. (2015) combined back-projections of 2D external forces to compute a 3D external force for an active contour based reconstruction method. Blondel et al. (2006) generated 3D reconstructions for every pair of multiple views and fused them together to find the final reconstruction. Liao et al. (2010) showed that, for back-projection based modelling, it is possible to integrate the information from multiple images using an elegant energy formulation for the correspondence. To this end, the authors formulated the problem not as a correspondence establishment but as a depth assignment to centrelines extracted from one of the projections. Li and Cohen (2011) and Jandt et al. (2009b) used modelling based on back-projection of vesselness response, which inherently supports multiple views. Finally, Keil et al. (2009) combined a geometric active contour model with a transformation to utilise all the images in a rotational X-ray angiography sequence.

Multi-view modelling could bring some advantages to the reconstruction. First, reconstruction methods that rely on only two projection images discard a significant amount of acquired images. Multi-view reconstruction benefits from extra information from the additional images, which improves the accuracy of the reconstruction (Cong et al., 2015; Liao et al., 2010). Second, two projection images are not enough for correspondence establishment between the projections if there is substantial amount of vessel overlap or foreshortening. In such cases, additional information from multiple views could assist the correspondence establishment (Liao et al., 2010). Finally, multiple images provide additional diameter measurements, which could be used to improve surface reconstruction (Cong et al., 2015; Movassaghi et al., 2004; Andriotis et al., 2008; Liao et al., 2010; Jandt et al., 2009b). However, necessity of manual processing from user may hinder the adoption of multi-view modeling. Therefore, it is important to invest on methods with minimal user interaction.

4.2.5. Vascular lumen reconstruction

Assessment of stenosis severity or simulations from 3D reconstruction of arteries demand not only the reconstruction of centrelines but also the reconstruction of arterial lumen walls (Fig. 9). Vessel surface reconstruction is performed after centreline reconstruction using the vessel diameter information from the projection images.

The basic approach to vessel surface reconstruction is to use vessel diameter information from only one view (Chen and Carroll, 2000; 2003; Cardenes et al., 2012; Liao et al., 2010). These methods extract the 2D diameter value by searching the vessel boundary perpendicular to vessel axis from one projection image. The diameter value is scaled to remove the scaling effect due to projection and the scaled diameter is used to fit a circle cross section perpendicular to the 3D vessel axis (Fig. 10a). These cross sections are used to create the surface of the coronary artery tree. Movassaghi et al. (2004) adapted this basic strategy to multi-view reconstruction. The scaled diameter values from multiple views put additional constraints on the shape of the vessel cross sections. Instead of limiting the cross sections to circles or ellipses, an interpolation scheme is proposed to accommodate various cross sections in Jandt et al. (2009b). To this end, the authors found the points that constrain the cross section and angularly interpolated new points describing the cross section. The interpolation is defined as a weighted linear combination and the weights are given based on a local foreshortening value and angular difference. Andriotis et al. (2008) observed that the plane where 3D circular cross section lies might not be perpendicular to 3D vessel axis due to the rotational movement of X-ray source (Fig. 10b). They proposed a strategy to extract diameter information using the plane of 3D circular cross section. Yang et al. (2009) proposed an ellipse fitting method for two views that respects non-coplanar circular cross sections in 3D. Later, (Cong et al., 2015) showed that this strategy can be incorporated into the multi-view reconstruction scenarios by using a least squares fitting.

Apart from reconstructing the vessel surface using the information available in the 2D angiography images, there is also a recent interest in fusing 3D centreline reconstructions with vessel surface extracted from IVUS or OCT images. Fig. 3 (Bruining et al., 2009; Reiber et al., 2011; Toutouzas et al., 2015). In this type of the vascular lumen reconstruction, 3D catheter path (Wahle et al., 1999) or 3D vessel centreline (Tu et al., 2010) is generally assumed to be reconstructed using X-ray images from a biplane system using a back-projection based method. The problem of vascular reconstruction is formulated in three steps: (i) segmentation of IVUS/OCT cross sections, (ii) identification of the centreline locations corresponding to ECG gated IVUS/OCT cross sections, and (iii) correction for the axial orientations of cross sections (Wahle et al., 1999; Bourantas et al., 2008; Tu et al., 2010; 2011; Doulaverakis et al., 2013). The spatial correspondence is established assuming an

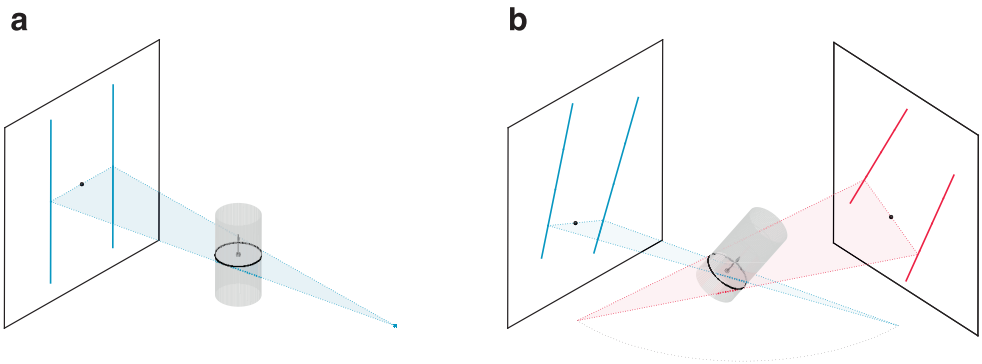

Fig. 10. Effect of C-arm movement on the vessel surface reconstruction: (a) Projection plane (light blue triangular area) is often assumed to be perpendicular to vessel axis. As a result, projection plane and vessel cross section (black circle) are parallel to each other. (b) If the movement of the C-arm is taken into account, projection plane (light blue triangular area) and vessel cross section (black circle) are no longer parallel to each other. Furthermore, projection planes from different views (light blue and red triangular area) are non-coplanar. (For interpretation of the references to color in this figure legend, the reader is referred to the web version of this article.)

initial correspondence and a constant pull-back speed (Wahle et al., 1999; Tu et al., 2010). The axial orientation correction is typically handled using local geometry around identified centreline points (Wahle et al., 1999; Bourantas et al., 2008; Tu et al., 2010; Doulaverakis et al., 2013).

4.3. Tomographic reconstruction

Tomographic reconstruction methods use X-ray coronary angiography images directly to produce a volume representing the coronary arteries. In contrast to binary representation of model-based reconstruction, tomographic reconstruction methods offer information about X-ray absorption coefficients. These methods can handle unusual anatomies (e.g. collaterals, tortuous branches) since they require less, if not none, prior information about the coronary arterial trees (Hansis et al., 2008d). Because of the same reason, these methods can also provide more accurate vessel surface details (Schoonenberg et al., 2009b). In addition, tomographic reconstruction methods do not require any manual interaction.

Tomographic reconstruction methods need to fulfil specific requirements. All of the tomographic reconstruction methods assume that the X-ray imaging system is calibrated prior to the acquisition. Compared with modeling based reconstruction, these methods generally demand more X-ray images with a larger angular coverage. For this reason, extended rotational X-ray angiography acquisition is preferred as the acquisition protocol (Table 2). However, one should note that even extended rotational X-ray angiography does not satisfy Tuy-Smith data sufficiency condition (Tuy, 1983; Smith, 1985). Moreover, as the coronary artery branches should be visible in the X-ray sequence, isocentring becomes crucial. Consistent contrast injection is also important to be able to exploit all the X-ray images. It is also important since these methods ignore the contrast agent propagation in their formulation and assume constant contrast distribution over time. Moreover, these methods typically have high computational demands compared with the modelling based reconstruction. However, thanks to the advances in parallel computing, dedicated GPU implementations can be used to overcome this difficulty (Table 3).

Similar to modelling methods, cardiac and respiratory motion are the most difficult challenges for the tomographic reconstruction. Typically, X-ray coronary angiography data are acquired during breath hold to minimise the respiratory motion. Depending on how they handle the cardiac motion, the tomographic reconstruction methods can be classified into three groups: (i) gated (Section 4.3.2), (ii) motion compensated (MC) (Section 4.3.3), and (iii) gated and motion compensated methods (Section 4.3.4). The basic considerations and algorithms for tomographic reconstruction are briefly introduced in Section 4.3.1. These algorithms are generally adapted to the specific problem of high contrast moving object reconstruction and specialised algorithms are proposed. A detailed discussion of specialised algorithms for coronary artery reconstruction is provided in Section 4.3.5. Background removal strategies are discussed in Section 4.3.6. Finally, a brief discussion on 3D+time (4D) tomographic reconstruction is given in Section 4.3.7.

4.3.1. Preliminaries

One distinction between different methods is the type of the tomographic reconstruction approach. Both analytical and iterative tomographic reconstruction algorithms have been developed.

Analytical reconstruction algorithms consider a simplified system model and image (volume) model. Thus, they are best suited to the situations where approximate solutions are adequate. Yet, these methods are well-established and fast compared to iterative alternatives. Popular choice for analytical reconstruction of cone-beam geometries is Feldkamp–Davis–Kress (FDK) (Feldkamp et al., 1984) algorithm.

Iterative reconstruction algorithms can integrate wide range of acquisition geometries (e.g. limited angular coverage), image model, forward model, noise model and prior information into the reconstruction (Hsieh et al., 2013). The image model mainly deals with the representation of the volume to be reconstructed. The continuous volume is approximated by a linear combination of basis functions at discrete regular rectangular grid locations (Hansis et al., 2009). Among alternatives, voxel (Blondel et al., 2004), Gaussian (Hansis et al., 2008c, 2008a), and blob-like (Kaiser–Bessel) (Zhou et al., 2008; Hu et al., 2010, 2012) basis functions are utilised[3]. The forward model describes the contribution of the voxels along X-ray line (or X-ray beam) to the corresponding pixels (Xu and Mueller, 2006). Although forward model should be explicit to increase reproducibility of the method, it is not always reported. This is most probably due to the fact that most of the methods use the length of intersection between X-ray lines and voxel grid image model. Unlike most other work, (Blondel et al., 2004) used the volume of the voxel if the X-ray beam is passing through the voxel. The image model and forward model can be combined to form an underdetermined system of linear equations (forward projection equations), which relate projected pixels and voxels to be reconstructed by a forward projection matrix. The lack of measurement error modelling in the forward projection equations is

[3] Unless otherwise noted, we assume that a voxel basis is used in the following discussion.

addressed by appropriate noise models. In the context of coronary artery reconstruction, Poisson (Zhou et al., 2008; Hu et al., 2010) or Gaussian (Hu et al., 2012) noise models are employed. Finally, the spatial dependency between neighbouring voxels can be used to include any prior information about the volume.

Iterative reconstruction algorithms are classified into two groups, namely algebraic and statistical. This classification is made on the basis of whether they account for a noise model or not. Both group of methods have been used in the context of coronary artery reconstruction.

4.3.2. Gated tomographic reconstruction

As with the modelling methods, one simple way to reduce the effect of motion on the reconstruction is to apply gating, i.e. select a subset of images that correspond to the same motion state of the coronary artery tree (Section 4.1.3).

The initial attempts to tomographic reconstruction from X-ray rotational X-ray angiography have focused on the feasibility and optimization of the acquisition protocols rather than the reconstruction method (Rasche et al., 2006b; Movassaghi et al., 2007). Because of this reason, these studies utilise analytical FDK type reconstruction algorithms with nearest-neighbour gating. On the other hand, cosine squared windowing function is shown to improve the reconstruction if an optimal window size is chosen (Schäfer et al., 2006). If the size of the window is increased, it possibly reduces the background artifacts but it leads to a blurred reconstruction due to motion (Schäfer et al., 2006). These motion corrupted reconstructions are not satisfactory for clinical purposes, however they can be benefited as an initial coarse reconstruction for a motion compensated reconstruction (Rohkohl et al., 2008a; 2009b; Schwemmer et al., 2013b, 2013a).

In recent years, the focus of gated reconstruction methods has shifted towards incorporation of prior information to cope with the undersampling due to gating. High contrast vessels occupy a small volume, therefore there must be a small number of voxels in the final reconstruction with nonzero voxel values (Li et al., 2002, 2004), assuming background pixels are removed from the X-ray images (see Section 4.3.6). Since it is not possible to embed prior information into analytical reconstruction algorithms, iterative reconstruction algorithms with some kind of sparsity prior have been proposed. In Li et al. (2004); Hansis et al. (2008c); Liu et al. (2014a), the forward projection equations are used as constraints and L1 norm of the reconstruction is minimised. Similarly, (Wu et al., 2011) minimised total variation (TV) norm of the reconstruction instead of L1 norm. Another way is to take a statistical approach and integrate the prior information in terms of a prior distribution model for the voxels. In particular, the voxel grid is considered a Markov Random Field (MRF) and the prior information is embedded using the clique potentials for the MRF. As the clique potentials, absolute value (Zhou et al., 2008) and sign functions (Hu et al., 2010, 2012) are used, which introduce TV-like and L0-like priors, respectively. An interesting way to introduce the prior information is to use a 3D centreline model. The prior probability for each voxel is defined as a function of the distance from a reference 3D centreline model to that voxel (Bousse Ast et al., 2009).

4.3.3. Motion compensated tomographic reconstruction

Since retrospective gating reduces the number of images available for the reconstruction, some reconstruction algorithms compensate for the effective motion instead of gating (Table 2). Essentially, the contributions from all X-ray images are brought to the same time point. Thus, all collected X-ray images are effectively used without introducing motion related artifacts. By means of a phantom coronary artery reconstruction experiment, (Schäfer et al., 2006) demonstrated that MC reconstruction can attain the quality of a static reconstruction from all projections, if the motion is known or estimated up to a certain accuracy. Therefore, the crucial part of every MC reconstruction algorithm is generally the motion estimation step.

MC methods require a representation of a motion field to model the mapping of the pixels or voxels from a reference time point to other time point. In general, the motion field is parameterised by a motion vector field or a geometric transformation. The temporal component of the motion field is commonly parameterised by cardiac phase assuming a periodic motion (Movassaghi et al., 2003; Blondel et al., 2006; Rohkohl et al., 2008a; Hansis et al., 2008d, 2009; Bousse Ast et al., 2009). However, the periodicity assumption is problematic for the cases where residual motion is strong or for the cases with arrhythmic heart motion (Rohkohl et al., 2009b). Because of this reason, the temporal component is sometimes parameterised by acquisition time (Rohkohl et al., 2009b, 2009a, 2010b). This strategy was shown to lead similar, if not superior, reconstructions.

Several types of geometric transformations have been investigated. A simplistic approach is to model the complex motion of the coronary arteries using 2D geometrical transformations acting on the X-ray images (Movassaghi et al., 2003; Hansis et al., 2008d). Two-dimensional rigid (Movassaghi et al., 2003) and 2D elastic (Hansis et al., 2008d) transformation are employed. Other studies use either 3D (Rohkohl et al., 2008a; Bousse Ast et al., 2009) or 4D (Blondel et al., 2006; Hansis et al., 2009; Rohkohl et al., 2009b, 2009a, 2010b) B-spline transformation. B-spline transformations offer spatial (and temporal if 4D) smoothness and achieve better results at the extent of an increase in the number of parameters to be estimated.

The parameters of the geometric transformation are estimated by an image registration method. For 2D transformations, an initial 3D reconstruction is obtained at a reference time and forward projected onto the projection images with a different time stamp. The parameter estimation problem is defined as estimating the registration between the features extracted from the projection images and the features extracted from forward projected images (Fig. 11a). 3D reconstructions of markers on the guidewire (Movassaghi et al., 2003) and ECG-gated tomographic reconstruction (Hansis et al., 2008d) are utilised to compute the forward projections. In some cases, the forward projected images are processed to extract some features (e.g. centrelines) for the registration (Hansis et al., 2008d). For 3D and 4D B-spline transformations, various strategies are proposed. One option is to propagate a 3D modelling based reconstruction to the remaining projection images (Section 4.2.3) (Blondel et al., 2006; Bousse Ast et al., 2009). Instead of a 3D modelling based reconstruction, a series of ECG-gated reconstructions can be obtained. These reconstructions are used to define an intensity based registration to estimate the parameters (Rohkohl et al., 2008a). Other possibility is to estimate the motion parameters jointly with the reconstruction (Fig. 11b) (Hansis et al., 2009; Rohkohl et al., 2009b, 2009a, 2010b). To achieve this goal, the parameters of the transformation are directly embedded into the analytical (Rohkohl et al., 2009b, 2009a, 2010b) or iterative (Hansis et al., 2009) reconstruction formulations. An energy functional is derived from these formulations with the addition of appropriate regularization term. The squared error between the projections of the reconstruction and X-ray images is used as the energy term in Hansis et al., 2009; Rohkohl et al., 2009a. Voxelwise multiplication of the reconstruction by a binarized reference 3D reconstruction is another alternative, which require a reference reconstruction (Rohkohl et al., 2009b, 2010b). Starting from an initial set of parameters and reconstruction, parameters are updated by a gradient based optimization and reconstruction is updated according to the reconstruction formula in an iterative manner.

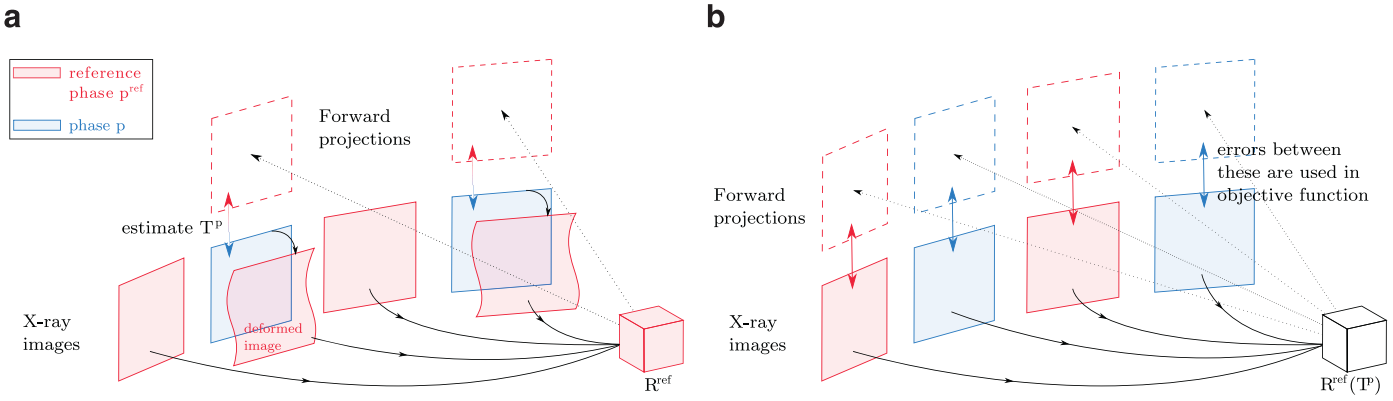

Fig. 11. Motion estimation strategies for motion compensated (MC) reconstruction: The motion is parameterised by an appropriate geometric transformation, T^p, and the parameters of the transformation are estimated by a registration process. R^{ref} and R^p denote initial reconstructions at a reference cardiac phase p_{ref} and at an arbitrary cardiac phase p, respectively. (a) For 2D geometric transformation, the motion estimation can be formulated as a registration between the X-ray images and the forward projection of R^{ref}. The 2D images at phase p are deformed according to the estimated transformation, and utilised in the reconstruction process. (b) For 3D geometric transformation, one option is to compute R^{ref} and T^p jointly. This is generally achieved by embedding the T^p into the reconstruction formulation and iteratively estimating R^{ref} and T^p by minimizing the error between the X-ray projections and forward projection of $R^{ref}(T^p)$.

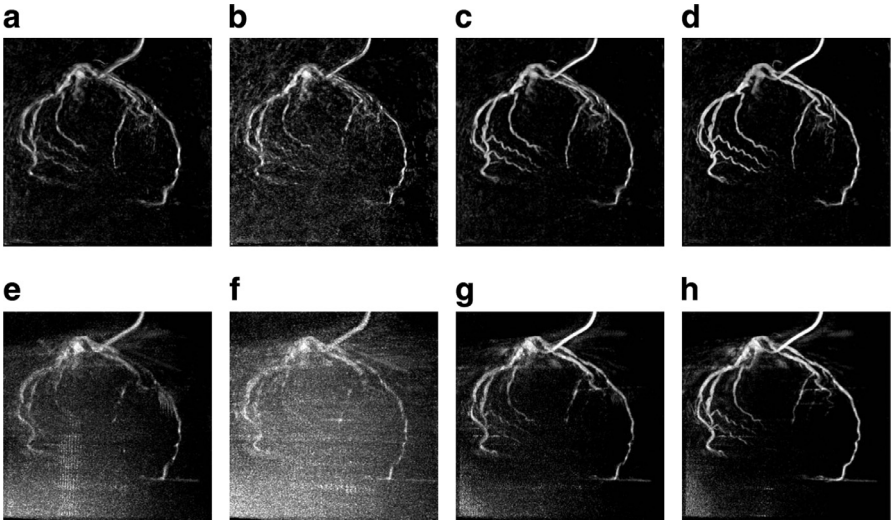

Fig. 12. An example of gated and motion compensated tomographic reconstruction: Top row, using 20% gating window: (a) reconstruction using FDK without motion compensation; (b) initial reconstruction using START; (c)–(d) reconstruction after first and second motion compensation cycle, respectively. Bottom row, using 40% gating window: (e) reconstruction using FDK without motion compensation. (b) initial reconstruction using START. (c)–(d) reconstruction after first and second motion compensation cycle, respectively. Reprinted from Hansis et al. (2010) with permission from AAPM.

The compensation for the estimated motion is mainly performed in two ways. First, the X-ray projection images are deformed using the estimated geometric transformation (Movassaghi et al., 2003; Hansis et al., 2008d). This is a trivial task if the estimated motion acts on pixels in 2D. On the other hand, if a 3D/4D motion field is estimated, it can be incorporated into the reconstruction formulation. Section 4.3.5 details how to achieve this for iterative (Blondel et al., 2004, 2006; Hansis et al., 2009; Bousse Ast et al., 2009) or analytical (Schäfer et al., 2006; Rohkohl et al., 2008a, 2009b, 2009a, 2010b, 2010a) formulations.

4.3.4. Gated and motion compensated tomographic Reconstruction

In gated tomographic reconstruction, the shape of the gating window is critical since it determines the trade-off between undersampling and motion artifacts (Schäfer et al., 2006). It is inevitable, however, to observe motion artifacts with a finite gating window due to residual motion (Hansis et al., 2008a). In some difficult circumstances, such as when the patient is unable to hold breath or in the presence of arrhythmic motion, motion artifacts are more severe (Rohkohl et al., 2010a). To improve this aspect of ECG-gated reconstruction methods, motion compensation strategies are proposed (Fig. 12) (Blondel et al., 2006; Hansis et al., 2008a, 2010; Rohkohl et al., 2010a; Schwemmer et al., 2013b, 2013a).

The gated MC methods typically parameterize the motion as a 2D geometric transformation (Blondel et al., 2006; Hansis et al., 2008d; Schwemmer et al., 2013b, 2013a). Two-dimensional elastic (Hansis et al., 2008d; 2010), a multiscale scheme of 2D affine and 2D B-spline (Schwemmer et al., 2013b, 2013a), and 2D translation (Blondel et al., 2006) are employed. The estimation of parameters are carried out by intensity based (Schwemmer et al., 2013b, 2013a) or feature based (e.g. centrelines) (Hansis et al., 2008d) registration between the forward projections of the ECG-gated reconstruction and X-ray images. The estimated transformation is applied on the projection images and these transformed images are used for the final MC reconstruction. In general, these methods compute the reconstruction and perform motion compensation in an iterative manner to reduce the effect of motion in the final reconstructions (Figure 12) (Hansis et al., 2010; Schwemmer et al., 2013a). Starting with a small gating windows and gradually increasing the size of the window as iterations progress is shown to be a reasonable strategy to deal with the

undersampling artifacts and motion at the same time (Schwemmer et al., 2013a).

As an alternative to 2D geometric transformation, Rohkohl et al. (2010a) employed 4D affine transformation to parameterise the residual motion. In particular, a set of temporal points are selected and assigned a 3D affine transform, from which the 3D affine transformation for the remaining time points are interpolated. The parameters of the affine transforms are estimated altogether and jointly with the gated reconstruction.

4.3.5. Specialised tomographic reconstruction algorithms

The fundamental tomographic reconstruction algorithms discussed in Section 4.3.1 mainly deal with the reconstruction of conventional CT. These algorithms are generally unsuitable for high contrast non-stationary coronary artery reconstruction because these may cause artifacts due to sparse high contrast vessels or undersampling due to gating. Moreover, modifications to these algorithms are required if motion compensation is intended. As a result, several specialised tomographic reconstruction algorithms are adapted from these basic algorithms.

Analytical FDK reconstruction algorithm is modified such that it copes with the undersampling due to retrospective gating (Movassaghi et al., 2007; Rohkohl et al., 2008a). A weighting factor is introduced to counteract the non-equidistant angular sampling (Movassaghi et al., 2007). Rohkohl et al. (2008a) observed actual low intensity voxels receive high contributions from some projection images, and this leads to streak artifacts. Thus, a novel weighting is devised to reduce the highest and lowest contributions for a voxel.

Some studies investigated the necessary modifications to FDK in order to convert it into a MC method. Schäfer et al. (2006) demonstrated how to incorporate motion into an analytical FDK reconstruction formulation. Their new formulation suggests that the filtering and back-projection steps must take the estimated motion vector field into account. However, the formulation does not take into account the effect of the motion vector field on the filtering in their implementation. In Rohkohl et al. (2009b, 2010b), the same MC-FDK formulation is used without ignoring the filtering step. This formulation is well-suited to the problems where motion and reconstruction are jointly estimated. Specifically, MC-FDK is inserted into an objective function and used multidimensional optimization to find the motion parameters and the reconstruction iteratively.

Iterative algebraic reconstruction algorithms are reformulated such that they benefit from sparse structure of the coronary arteries. Instead of directly solving the forward projection equations, L1 norm of the reconstruction is minimised with the forward project equations used as constraints (Li et al., 2002, 2004; Hansis et al., 2008c). By introducing a quadratic perturbation term, the minimization problem can be approximated and efficiently solved via an iterative scheme, which is akin to the conventional ART (Li et al., 2004). Intuitively, nonzero constraint of original ART is relaxed and the solution space is enriched by addition of new subspaces (Hansis et al., 2008c). This effect is mainly due to a voxel-wise thresholding in the new formulation. Therefore, the algorithm is called thresholded ART (TART). Hansis et al. (2008c) proposed simultaneous TART (START) technique following the similar changes to convert ART to SART. Recently Liu et al. (2014a) combined START with a novel background removal technique (Section 4.3.6).

Incorporation of the motion into iterative algebraic reconstruction formulation is studied in Blondel et al. (2004). The authors showed that the forward projection matrix can be represented such that it depends on the estimated motion vector field. Their formulation states that the entries of the forward projection matrix are given by the volume of the intersection of the X-ray beam with the deformed voxel. After calculation of the forward projection matrix, any iterative algebraic technique can be utilised for the reconstruction. A similar formulation with a generic image model and X-ray lines are presented in Hansis et al. (2009). Calculation of forward projection matrix is computationally expensive and approximations are made (Blondel et al., 2004; Hansis et al., 2009).

Other methods based on joint estimation-reconstruction or iterative statistical reconstruction algorithms generally employ well-known energy minimization algorithms. These algorithms are used without any modifications, however we mention these algorithms in this section for completeness. Alternatives for energy minimization include gradient descent (Hansis et al., 2009), stochastic gradient descent (Rohkohl et al., 2009a, 2010a), L-BFGS-B (Rohkohl et al., 2009b, 2010b), separable paraboloidal surrogates (SPS) (Erdogan and Fessler, 1999; Hu et al., 2010, 2012), and block sequential regularized expectation maximization (BSREM) (de Pierro and Beleza Yamagishi, 2001; Zhou et al., 2008).

4.3.6. Background removal

X-ray coronary angiography not only includes coronary arteries but also background structures such as spine, ribs or diaphragm. These background structures may cause truncation errors because they are not visible in all projection images due to field of view (Blondel et al., 2006). In addition, the background structures may hinder the use of sparsity as a prior information (Hansis et al., 2008c). As a result, most of the tomographic reconstruction methods require background removal from X-ray images as a preprocessing or an intermediate step.

Simple image processing techniques are commonly utilised for background removal. The most popular choice is to apply a top-hat filter (Soille, 2004) to suppress the background (Hansis et al., 2008d, 2008c, 2008a, 2009; Rohkohl et al., 2010a; Liu et al., 2014a). A good suppression can be achieved, however the size of the filter may effect the results (Liu et al., 2014a). On the other hand, some segmentation based background removal algorithms are proposed (Blondel et al., 2006; Zhou et al., 2008; Hu et al., 2010, 2012; Schwemmer et al., 2013b). These methods first segment the coronary arteries from X-ray images and remove corresponding pixels. These pixels are filled with intensity value estimates from neighbouring background structures to obtain a background image. Hysteresis thresholding of tubularity image (Blondel et al., 2006; Zhou et al., 2008), thresholding of top-hat filtered image (Hu et al., 2010; Schwemmer et al., 2013b), and level set based segmentation (Hu et al., 2012) are employed. To fill the removed pixels, morphological closure (Blondel et al., 2006; Zhou et al., 2008) and image inpainting (Hu et al., 2012) are used.

Some reconstruction methods perform background subtraction during the reconstruction. In Rohkohl et al. (2009b, 2010b), a thresholded reference reconstruction is integrated into reconstruction formulation to reduce the effect of the background structures on the optimization. On the other hand, (Liu et al., 2014a) proposed to segment intermediate reconstruction of the iterative reconstruction algorithm and used forward projections of the segmentation to suppress background structures on the X-ray images.

The background is generally suppressed or subtracted from the X-ray projection images. This strategy is problematic for iterative statistical reconstruction algorithms since the distribution of the subtraction image does not follow the original assumption (Zhou et al., 2008). In such cases, integration of background estimation into statistical model improves the reconstruction quality (Zhou et al., 2008).

4.3.7. 3D+time (4D) tomographic reconstruction

The simplest way to obtain 3D+time (4D) tomographic reconstruction is to reconstruct for a number of time points independently (Fig. 13) (Movassaghi et al., 2007; Hansis et al., 2010). However, it may be impossible to attain the same level of accuracy in

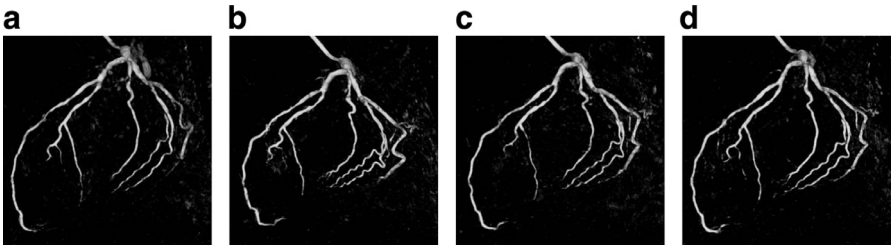

Fig. 13. An example of 4D tomographic reconstruction: volume renderings of reconstructions of a left coronary artery at (a) 0%, (b) 25%, (c) 50%, (d) 75% of the cardiac cycle. Reprinted from Hansis et al. (2010) with permission from AAPM.

different time points due to several factors (e.g. residual motion related to gating window size). In addition, the motion of the arteries can not be studied quantitatively (Holub et al., 2011). To overcome these limitations, Holub et al. (2011) proposed a strategy to exploit the motion estimated for a MC reconstruction method. Because the parameterisation of the motion is from arbitrary time points to a reference time points, an energy minimization is proposed to inverse the estimated motion vector field. Inverse motion vector field is used to transform the best-quality reconstruction to the other time points. Unlike this strategy, the methods that perform joint reconstruction and motion estimation can directly deliver the 4D reconstruction result (Hansis et al., 2009).

5. Evaluation methods for coronary artery reconstructions

Comparison between different types of the coronary artery reconstruction methods is difficult to achieve due to diversity of the acquisition protocols, specific requirements for the method (e.g. ECG, calibration, user interaction), and especially the lack of standard dataset and performance metrics. Nevertheless, common evaluation types (Section 5.1), phantom datasets (Section 5.2) and evaluation metrics (Section 5.3) can be identified from the relevant literature to provide insight into the efforts towards a standardised quantitative comparison.

5.1. Evaluation type

Three main groups of evaluation types can be distinguished: qualitative results, quantitative with phantom experiments, and quantitative with experiments on real patient data (Table 3).

The methods with qualitative evaluation visually compare the results with the results from other methods to provide evidence of the feasibility of the method. These methods are rare in the literature, especially within the journal publications. Further assessment of these methods are required to determine their strengths and weaknesses.

Quantitative evaluations are performed by experiments employing either phantom data or real patient data.

5.2. Phantom datasets

The ground truth required for the validation is not directly available for the reconstruction problem. One way to address this issue is to utilise physical and software phantoms where the ground truth is known.

Physical phantoms are advantageous in terms of exposing the reconstruction methods to the practical limitations of image acquisition. However, they tend to be limited to simple motion models, since it is hard to imitate the complex combination of cardiac and respiratory motion. In addition, ground truth information must be extracted from a stationary reconstruction of the phantom usually based on manual or semi-automatic image segmentation.

Several physical phantoms with different levels of complexity have been used. Wire (Hoffmann et al., 2000; Cañero et al., 2002) and guide-wire (Chen and Carroll, 2000) phantoms are primitive examples. A 3D-printed static bifurcation and stenosis phantom is used in Yang et al., 2009. The ground truth is determined from the geometric description of the object. In Movassaghi et al. (2004), a stenotic coronary artery phantom is used. A static coronary artery phantom with realistic topology is used in Liao et al. (2010). The phantom is scanned with multislice CT (MSCT) and segmented to find the ground truth centrelines. Shechter et al. (2003a) used contrast filled tubes over a compliant latex balloon to mimic the motion. The motion is controlled with mechanical inflation of the balloon. The ground-truth is obtained by segmenting a gated multislice MR of the object and identifying the temporal correspondences between ground-truth and X-ray acquisition. A similar artificial heart and coronary phantom is proposed in Rohkohl et al. (2009b, 2010b). The authors placed tubular structures filled with contrast over an elastic material filled with water. The cardiac motion is controlled with a pump that pushes water in an out, and the respiratory motion is controlled with specialised hardware. Jandt et al. (2009b) used a commercially available complex chest phantom (Radiology Support Devices, 2006).

Software phantoms offer flexible environments for the reconstruction experiments. These phantoms can simultaneously take into account several factors such as the complex topology of vessels, cardiac and heart motions. However, imaging geometry and physics of image acquisition are often simplified.

Lorenz et al. (2004) built a software phantom from a mean model of the coronary artery trees adapted from the clinical information provided in Dodge et al. (1992). The motion of the arteries are included using affine transformations between cardiac phases (Schäfer et al., 2006). Yang et al. (2007, 2012) built a phantom from MSCT data to obtain a more realistic results. They segmented the coronary arteries from MSCT and set the segmented voxel values to a high value to simulate contrast injection. Another possibility is to exploit the coronary artery anatomical model in the 4D XCAT phantom (Segars et al., 2010). Fung et al. (2011) generated more complete anatomical model for XCAT, based on morphometric and physiological rules. Rohkohl et al. (2010c) used XCAT phantom to generate realistic X-ray rotational angiography images. In fact, this work constitutes the first attempt to define a standardised quantitative comparison platform. The projection images and relevant additional information are publicly available. Any voxelized reconstruction result can be submitted to the platform for evaluation and ranking.

5.3. Evaluation metrics

The reconstruction results are qualitatively assessed via evaluation metrics measuring the similarity of the reconstruction and the ground truth. Depending on the reconstruction method and the ground truth information various evaluation metrics have been proposed.

Evaluation metrics for model-based reconstruction methods are based on ground truth centreline. To emphasise robustness of the method against foreshortening, the difference between the length of the ground truth and reconstructed centreline is typically preferred for the experiments with wire phantom (Chen and Carroll, 2000; Cañero et al., 2002; Chen and Carroll, 2003). Angles of specific bifurcations are also used to define an error measure (Chen and Carroll, 2003; Andriotis et al., 2008). Apart from these metrics, the most common metrics are 2D reprojection error and 3D space error. The 2D reprojection error is used to quantitatively evaluate the performance in the experiments using clinical X-ray angiography images. It is defined using the Euclidean distance between the manually segmented ground truth centrelines from the X-ray images and forward projection of the reconstructed arteries onto the 2D detector plane. However, it is demonstrated in Cong et al. (2015) that 2D reprojection error does not correlate well with the 3D space error . Therefore, the 2D reprojection error must be calculated from projection angles that are not included in the reconstruction or favourably supported by appropriate 3D evaluation metric. The 3D space error is used in the experiments where the 3D ground truth is available and is generally considered most conclusive centreline based metric. It is simply defined using the 3D Euclidean distance between the reconstruction and the ground truth.

Surface or attenuation coefficient based metrics are proposed for tomographic reconstruction methods. Mean radius error (Rohkohl et al., 2010b) or mean relative radius error (Hansis et al., 2008d, 2008c; Liu et al., 2014a) are calculated from the planes whose normal is the ground truth centreline. Another metric is defined as the fraction of the energy (integral of voxel values) located inside the ground truth surface (Hansis et al., 2008d). Similar to this metric, RMS error or MSE of voxel values over whole volume or near coronary artery centrelines are employed (Schäfer et al., 2006; Hansis et al., 2008c; Zhou et al., 2008; Hansis et al., 2010; Hu et al., 2010). These attenuation value metrics are reasonable indicators of the contrast and artifact in the resulting reconstruction. Another way of assessing the image artifacts is to employ a noise estimator (Schwemmer et al., 2013b). Another popular choice for assessment is to compare a thresholded reconstruction with the binary ground truth. Recall rate (Bousse Ast et al., 2009) or Dice coefficient (Hu et al., 2012) are utilised. In Rohkohl et al. (2010c), a set of thresholds are used to convert reconstruction into binary volumes and the maximum Dice coefficient is assigned as the quality metric. This metric can work with modelling based reconstructions if the voxelization of the reconstruction is supplied.

There is also some interest in eliminating necessity of having a ground truth. For this purpose, sharpness metric is adapted in Schwemmer et al. (2013b, 2014). The centreline is semi-automatically extracted from the reconstructed image and intensity profiles perpendicular to the centrelines are computed. The metric is defined as the inverse of the average distance between the point of 80% and 20% decrease along the intensity profiles. An implementation of this metric is available as a part of a multi-modality 3D coronary artery reconstruction evaluation software (Schwemmer et al., 2014).

6. Discussion and conclusions

During the last decade, healthcare has witnessed tremendous advances in the coronary artery imaging technologies. Three main directions of development efforts can be distinguished: (i) development of non-invasive diagnostic imaging technologies, such as MRA and CCTA, (ii) development of non-invasive interventional technologies, such as C-arm CBCT, and (iii) development of invasive interventional technologies, such as IVUS, OCT and X-ray coronary angiography. In the current situation, there is a competition between some of these imaging techniques to determine the most effective areas of use for particular imaging technology. However, it is clear that no single imaging technique can overthrow the others, since they all have different advantages and limitations. Therefore, it is crucial to identify the potential of the each imaging modality and to dedicate imaging and clinical research to each of those to improve all technologies simultaneously.

Advances in the non-invasive imaging modalities do not necessarily result in a decline of the invasive technologies. However, several aspects of clinical decision making, which now depends on X-ray coronary angiography and reconstructions obtained from it, can be effectively handled by a more appropriate imaging modality. The main competitor of X-ray coronary angiography is CCTA. It is anticipated that the CCTA will be the dominant imaging modality for the selection of patients for PCI and the intervention planning due to its non-invasiveness. However, several important factors must be considered before adoption of this technology, such as patient radiation dose, practice guidelines and financial issues (Mark et al., 2010). In this regard, X-ray coronary angiography is an established imaging modality, and it is expected to remain as the main imaging modality for the guidance during the interventions. In order to fully exploit X-ray coronary angiography capabilities, 3D/4D reconstruction from X-ray coronary angiography should make its way to the intervention room.

Reconstruction from X-ray coronary angiography can facilitate PCI in several ways. In fact, 3D/4D reconstructions are progressively being integrated into PCI. Optimal view selection using reconstructions is a remarkable example of these integration efforts. Optimal views obtained without additional radiation or contrast can help with the stent positioning (Green et al., 2005; Eng et al., 2013). In a similar fashion, tomographic reconstructions can be used to simulate intracoronary images to provide further guidance for stent positioning (Schoonenberg et al., 2009b). Furthermore, live overlay of the reconstruction on the fluoroscopy images can provide navigational guidance and possibly lead to a reduction in the contrast material use (Schoonenberg et al., 2009a). In the near future, dynamic reconstructions and holographic imaging can provide a truly 3D display for the understanding of the spatial structure of the coronary arteries.

Fusion of different imaging modalities to exploit supplementary information is another promising direction for the future of X-ray coronary angiography. In this context, reconstructions from X-ray coronary angiography can be utilised instead of raw images. Extracted information from diagnostic CCTA scans can be overlaid with reconstructions to bring the pre-operative planning into the cath-lab (Dibildox et al., 2014). Fusion of reconstructions with IVUS or OCT can provide useful information concerning the morphological information about the stenosis and wall characteristics (Bruining et al., 2009). Moreover, combination of TEE with 4D reconstructions can supply valuable soft-tissue information (Rasche et al., 2008). Most importantly, information from functional imaging techniques must be fused with the anatomical information of the reconstructions. This is one of the directions that requires a special attention in the future.

An intriguing direction for the future research is the investigation of the tomosynthesis capability of the existing X-ray coronary angiography systems for high-contrast vascular structure reconstruction (Langan et al., 2015). In fact, this can be considered the natural next step for tomographic coronary artery reconstruction from extended rotational X-ray angiography. Successful results can lead to reduction in the radiation dose and may result in the change of the acquisition protocol, analogous to the transition from conventional to (dual-axis) rotational angiography.

Novel and robust clinical tools are required to strengthen X-ray coronary angiography's position inside cath-lab. Improvements on

virtual FFR estimation (Morris et al., 2013; Papafaklis et al., 2014; Tu et al., 2014; Morris et al., 2015) or virtual stenting (Larrabide et al., 2012) could make these technologies available for intraoperative decision making. Real-time simulation of deployment of stent deployment and computation of the resulting hemodynamic changes by the help of 3D/4D reconstructions can be set as the next targets for clinical tool development.

To achieve the ambitious goals stated above, several aspects of the current reconstruction methods must be reconsidered. First, the manual interaction required for most of the modeling based reconstructions hinders clinical translation of these methods for real-time processing (Table 1). Almost automated methods are essential to make reconstruction technology as an irreplaceable part of cath-lab. Second, the time requirement of the methods should be reduced to the order of seconds by the help of modern parallel computing opportunities (Table 3). The recent progress on this direction is encouraging and shows the feasibility of online processing inside cath-lab (Eng et al., 2013). Third, 4D reconstruction methods with reasonable time requirements should be devised to fully exploit the capabilities of X-ray coronary angiography. Finally, a grand challenge could be organised to be able to overcome the lack of comparability in 3D/4D reconstruction research. Initial endeavour to generate a publicly available database for comparison (Rohkohl et al., 2010c) is a notable step toward this direction. A broader quantitative evaluation should involve validation by appropriate metrics capable of providing 3D/4D errors on three possible levels, namely, software phantom, physical phantom and clinical images.

Acknowledgments

Serkan Çimen holds a Ph.D. scholarship from the Department of Electronic and Electrical Engineering, The University of Sheffield, UK. This study was partially supported by Wellcome Trust Health Innovation Challenge Fund (grant HICF-R6-365).

References

Agostoni, P., Biondi-Zoccai, G., Van Langenhove, G., Cornelis, K., Vermeersch, P., Convens, C., Vassanelli, C., Van Den Heuvel, P., Van Den Branden, F., Verheye, S., 2008. Comparison of assessment of native coronary arteries by standard versus three-dimensional coronary angiography. Am. J. Cardiol. 102 (3), 272–279.

Andriotis, A., Zifan, A., Gavaises, M., Liatsis, P., Pantos, I., Theodorakakos, A., Efstathopoulos, E.P., Katritsis, D., 2008. A new method of three-dimensional coronary artery reconstruction from X-ray angiography: Validation against a virtual phantom and multislice computed tomography. Catheter. Cardiovasc. Interv. 71 (1), 28–43.

Baka, N., Metz, C.T., Schultz, C., Neefjes, L., van Geuns, R.J., Lelieveldt, B.P.F., Niessen, W.J., van Walsum, T., de Bruijne, M., 2013. Statistical coronary motion models for 2D+t/3D registration of X-ray coronary angiography and CTA. Med. Image Anal. 17 (6), 698–709.

Blondel, C., Malandain, G., Vaillant, R., Ayache, N., 2006. Reconstruction of coronary arteries from a single rotational X-ray projection sequence. IEEE Trans. Med. Imaging 25 (5), 653–663.

Blondel, C., Vaillant, R., Malandain, G., Ayache, N., 2004. 3D tomographic reconstruction of coronary arteries using a precomputed 4D motion field. Phys. Med. Biol. 49 (11), 2197–2208.

Bouattour, S., Arndt, R., Paulus, D., 2005. 4D reconstruction of coronary arteries from monoplane angiograms. In: Proceedings of the Computer Analysis and Images Patterns. Springer Berlin Heidelberg, pp. 724–731.

Bourantas, C.V., Kalatzis, F.G., Papafaklis, M.I., Fotiadis, D.I., Tweddel, A.C., Kourtis, I.C., Katsouras, C.S., Michalis, L.K., 2008. ANGIOCARE: An automated system for fast three-dimensional coronary reconstruction by integrating angiographic and intracoronary ultrasound data. Catheter. Cardiovasc. Interv. 72 (2), 166–175.

Bousse Ast, A., Zhou, J., Yang, G., Bellanger, J.-J., Toumoulin, C., 2009. Motion compensated tomography reconstruction of coronary arteries in rotational angiography.. IEEE Trans. Biomed. Eng. 56 (4), 1254–1257.

Bruining, N., de Winter, S., Serruys, P.W., 2009. Intravascular ultrasound registration/integration with coronary angiography. Cardiol. Clin. 27 (3), 531–540.

Cañero, C., Radeva, P., Toledo, R., Villanueva, J., Mauri, J., 2000. 3D curve reconstruction by biplane snakes. In: Proceedings of the IEEE International Conference on Pattern Recognition. IEEE, pp. 563–566.

Cañero, C., Vilariño, F., Mauri, J., Radeva, P., 2002. Predictive (un)distortion model and 3-D reconstruction by biplane snakes. IEEE Trans. Med. Imaging 21 (9), 1188–1201.

Calmac, L., Niculescu, R., Badila, E., Weiss, E., Zamfir, D., Itu, L., Lazar, L., Carp, M., Itu, A., Suciu, C., Passerini, T., Sharma, P., Georgescu, B., Comaniciu, D., 2015. TCT-40 image-based computation of instantaneous wave-free ratio from routine coronary angiography - initial validation by invasively measured coronary pressures. J. Am. Coll. Cardiol. 66 (15), B17–B18.

Campbell, P.T., Mahmud, E., 2014. TCT-84 prospective, online, interactive survey comparing visual lesion estimation to quantitative coronary angiography. J. Am. Coll. Cardiol. 64 (11), B25.

Cardenes, R., Novikov, A., Gunn, J., Hose, R., Frangi, A.F., 2012. 3D reconstruction of coronary arteries from rotational X-ray angiography. In: Proceedings of the IEEE International Symposium Biomedical Imaging. IEEE, pp. 618–621.

Carroll, J.D., Carroll, E.P., Chen, S.J., 2009. Coronary angiography: the need for improvement and the barriers to adoption of new technology. Cardiol. Clin. 27 (3), 373–383.

Çimen, S., Hoogendoorn, C., Morris, P., Gunn, J., Frangi, A., 2014. Reconstruction of coronary trees from 3DRA using a 3D+t statistical cardiac prior. In: Golland, P., Hata, N., Barillot, C., Hornegger, J., Howe, R. (Eds.), Proceedings of the Medical Image Computing and Computer-Assisted Intervention. Springer International Publishing, pp. 619–626.

Chen, S.J., Carroll, J.D., 2000. 3-D reconstruction of coronary arterial tree to optimize angiographic visualization. IEEE Trans. Med. Imaging 19 (4), 318–336.

Chen, S.J., Schäfer, D., 2009. Three-dimensional coronary visualization, Part 1: modeling.. Cardiol. Clin. 27 (3), 433–452.

Chen, S.Y.J., Carroll, J.D., 2003. Kinematic and deformation analysis of 4-D coronary arterial trees reconstructed from cine angiograms.. IEEE Trans. Med. Imaging 22 (6), 710–721.

Cohen, L., Cohen, I., 1993. Finite-element methods for active contour models and balloons for 2-D and 3-D images. IEEE Trans. Pattern Anal. Mach. Intell. 15 (11), 1131–1147.

Cong, W., Yang, J., Ai, D., Chen, Y., Liu, Y., Wang, Y., 2015. Quantitative analysis of deformable model-based 3-D reconstruction of coronary artery from multiple angiograms. IEEE Trans. Biomed. Eng. 62 (8), 2079–2090.

Cong, W., Yang, J., Liu, Y., Wang, Y., 2013. Energy back-projective composition for 3-D coronary artery reconstruction.. Proc. IEEE Eng. Med. Biol. Soc. 2013, 5151–5154.

Dibildox, G., Baka, N., Punt, M., Aben, J.-P., Schultz, C., Niessen, W., van Walsum, T., 2014. 3D/3D registration of coronary CTA and biplane XA reconstructions for improved image guidance.. Med. Phys. 41 (9), 091909.

Dodge, J.T., Brown, B.G., Bolson, E.L., Dodge, H.T., 1992. Lumen diameter of normal human coronary arteries. Influence of age, sex, anatomic variation, and left ventricular hypertrophy or dilation. Circulation 86 (1), 232–246.

Doulaverakis, C., Tsampoulatidis, I., Antoniadis, A.P., Chatzizisis, Y.S., Giannopoulos, A., Kompatsiaris, I., Giannoglou, G.D., 2013. IVUSAngio tool: a publicly available software for fast and accurate 3D reconstruction of coronary arteries.. Comput. Biol. Med. 43 (11), 1793–1803.

Dvir, D., Assali, A., Kornowski, R., 2008. Percutaneous coronary intervention for chronic total occlusion: Novel 3-dimensional imaging and quantitative analysis. Catheter. Cardiovasc. Interv. 71 (6), 784–789.

Eng, M.H., Hudson, P.A., Klein, A.J., Chen, S.J., Kim, M.S., Groves, B.M., Messenger, J.C., Wink, O., Carroll, J.D., Garcia, J.A., 2013. Impact of three dimensional in-room imaging (3DCA) in the facilitation of percutaneous coronary interventions. J. Cardiol. Vasc. Med. 1 (1), 1–5.

Erdogan, H., Fessler, J.A., 1999. Ordered subsets algorithms for transmission tomography.. Phys. Med. Biol. 44 (11), 2835–2851.

Fahrig, R., Fox, A.J., Lownie, S., Holdsworth, D.W., 1997. Use of a C-arm system to generate true three-dimensional computed rotational angiograms: preliminary in vitro and in vivo results.. Am. J. Neuroradiol. 18 (8), 1507–1514.

Fallavollita, P., Cheriet, F., 2008. Optimal 3D reconstruction of coronary arteries for 3D clinical assessment.. Comput. Med. Imaging Graph. 32 (6), 476–487.

Feldkamp, L.A., Davis, L.C., Kress, J.W., 1984. Practical cone-beam algorithm. J. Opt. Soc. Am. 1 (6), 612.

Fung, G.S.K., Segars, W.P., Gullberg, G.T., Tsui, B.M.W., 2011. Development of a model of the coronary arterial tree for the 4D XCAT phantom. Phys. Med. Biol. 56 (17), 5651–5663.

Garcia, J., Movassaghi, B., Casserly, I., Klein, A., James Chen, S.-Y., Messenger, J., Hansgen, A., Wink, O., Groves, B., Carroll, J., 2009. Determination of optimal viewing regions for X-ray coronary angiography based on a quantitative analysis of 3D reconstructed models. Int. J. Cardiovasc. Imaging 25 (5), 455–462.

Garcia, J.A., Chen, J., Hansgen, A., Wink, O., Movassaghi, B., Messenger, J.C., 2007. Rotational angiography (RA) and three-dimensional imaging (3-DRA): an available clinical tool. Int. J. Cardiovasc. Imaging 23 (1), 9–13.

Go, A.S., Mozaffarian, D., Roger, V.L., Benjamin, E.J., Berry, J.D., Blaha, M.J., Dai, S., Ford, E.S., Fox, C.S., Franco, S., Fullerton, H.J., Gillespie, C., Hailpern, S.M., Heit, J.a., Howard, V.J., Huffman, M.D., Judd, S.E., Kissela, B.M., Kittner, S.J., Lackland, D.T., Lichtman, J.H., Lisabeth, L.D., Mackey, R.H., Magid, D.J., Marcus, G.M., Marelli, A., Matchar, D.B., McGuire, D.K., Mohler, E.R., Moy, C.S., Mussolino, M.E., Neumar, R.W., Nichol, G., Pandey, D.K., Paynter, N.P., Reeves, M.J., Sorlie, P.D., Stein, J., Towfighi, A., Turan, T.N., Virani, S.S., Wong, N.D., Woo, D., Turner, M.B., 2014. Heart Disease and Stroke Statistics - 2014 Update: A report from the American Heart Association. Circulation 129 (3), e28–e292.

Gollapudi, R.R., Valencia, R., Lee, S.S., Wong, G.B., Teirstein, P.S., Price, M.J., 2007. Utility of three-dimensional reconstruction of coronary angiography to guide percutaneous coronary intervention. Catheter. Cardiovasc. Interv. 69 (4), 479–482.

Green, N.E., Chen, S.-Y. J., Hansgen, A.R., Messenger, J.C., Groves, B.M., Carroll, J.D., 2005. Angiographic views used for percutaneous coronary interventions: A three-dimensional analysis of physician-determined vs. computer-generated views. Catheter. Cardiovasc. Interv. 64 (4), 451–459.

Green, N.E., Chen, S.-Y. J., Messenger, J.C., Groves, B.M., Carroll, J.D., 2004. Three-dimensional vascular angiography.. Curr. Probl. Cardiol. 29 (3), 104–142.

Hansis, E., Carroll, J.D., Schäfer, D., Dössel, O., Grass, M., 2010. High-quality 3-D coronary artery imaging on an interventional C-arm x-ray system.. Med. Phys. 37 (4), 1601–1609.

Hansis, E., Dossel, O., Grass, M., 2008a. Motion-compensated iterative sparse data reconstruction for interventional 3-D coronary artery imaging. In: Proceedings of the IEEE Nuclear Science Symposium Conference Record.. IEEE, pp. 4280–4284.

Hansis, E., Schäfer, D., Dössel, O., Grass, M., 2008b. Automatic optimum phase point selection based on centerline consistency for 3D rotational coronary angiography. Int. J. Comput. Assist. Radiol. Surg. 3 (3–4), 355–361.

Hansis, E., Schäfer, D., Dössel, O., Grass, M., 2008c. Evaluation of iterative sparse object reconstruction from few projections for 3-D rotational coronary angiography.. IEEE Trans. Med. Imaging 27 (11), 1548–1555.

Hansis, E., Schäfer, D., Dössel, O., Grass, M., 2008d. Projection-based motion compensation for gated coronary artery reconstruction from rotational x-ray angiograms.. Phys. Med. Biol. 53 (14), 3807–3820.

Hansis, E., Schomberg, H., Erhard, K., Dössel, O., Grass, M., 2009. Four-dimensional cardiac reconstruction from rotational x-ray sequences: first results for 4D coronary angiography. In: Proceedings of the SPIE. SPIE. pp. 72580B–72580B–11. doi: 10.1117/12.811104.

Hartley, R., Zisserman, A., 2004. Multiple View Geometry in Computer Vision, second ed. Cambridge University Press.

Hetterich, H., Redel, T., Lauritsch, G., Rohkohl, C., Rieber, J., 2010. New X-ray imaging modalities and their integration with intravascular imaging and interventions. Int. J. Cardiovasc. Imaging 26 (7), 797–808.

Hoffmann, K., Sen, A., Lan, L., Chua, K.-G., Esthappan, J., Mazzucco, M., 2000. A system for determination of 3D vessel tree centerlines from biplane images. Int. J. Card. Imaging 16 (5), 315–330.

Holub, W., Rohkohl, C., Schuldhaus, D., Prümmer, M., Lauritsch, G., Hornegger, J., 2011. 4D motion animation of coronary arteries from rotational angiography. In: Proceedings of the SPIE. SPIE. pp. 79641S–79641S–10. doi: 10.1117/12.877969.

Hsieh, J., Nett, B., Yu, Z., Sauer, K., Thibault, J.-B., Bouman, C., 2013. Recent advances in CT image reconstruction. Curr. Radiol. Rep. 1 (1), 39–51.

Hu, Y., Jung, M., Oukili, A., Yang, G., Nunes, J.-C., Fehrenbach, J., Peyre, G., Bedossa, M., Luo, L., Toumoulin, C., Cohen, L.D., 2012. Sparse reconstruction from a limited projection number of the coronary artery tree in X-ray rotational imaging. In: Proceedings of the IEEE International Symposium on Biomedical Imaging. IEEE, pp. 804–807.

Hu, Y., Xie, L., Nunes, J.C., Bellanger, J.J., Bedossa, M., Toumoulin, C., 2010. ECG gated tomographic reconstruction for 3-D rotational coronary angiography. In: Proceedings of the IEEE Engineering in Medicine and Biology Society. IEEE, pp. 3614–3617.

Hui, Z., Friedman, M., 2002. Tracking 3-D coronary artery motion with biplane angiography. In: Proceedings of the IEEE International Symposium on Biomedical Imaging. IEEE, pp. 605–608.

Husmann, L., Leschka, S., Desbiolles, L., Schepis, T., Gaemperli, O., Seifert, B., Cattin, P., Frauenfelder, T., Flohr, T.G., Marincek, B., Kaufmann, P.A., Alkadhi, H., 2007. Coronary artery motion and cardiac phases: dependency on heart rate – implications for CT image reconstruction. Radiology 245 (2), 567–576.

Jandt, U., Schäfer, D., Grass, M., Rasche, V., 2009a. Automatic generation of 3D coronary artery centerlines using rotational X-ray angiography.. Med. Image Anal. 13 (6), 846–858.

Jandt, U., Schäfer, D., Grass, M., Rasche, V., 2009b. Automatic generation of time resolved motion vector fields of coronary arteries and 4D surface extraction using rotational x-ray angiography. Phys. Med. Biol. 54 (1), 45–64.

Johnson, N.P., Kirkeeide, R.L., Gould, K.L., 2013. Coronary anatomy to predict physiology: fundamental limits.. Circ. Cardiovasc. Imaging 6 (5), 817–832.

Kachelriess, M., Ulzheimer, S., Kalender, W.A., 2000. ECG-correlated imaging of the heart with subsecond multislice spiral CT.. IEEE Trans. Med. Imaging 19 (9), 888–901.

Kass, M., Witkin, A., Terzopoulos, D., 1988. Snakes: Active contour models. Int. J. Comput. Vis. 1 (4), 321–331.

Keil, A., Vogel, J., Lauritsch, G., Navab, N., 2009. Dynamic cone beam reconstruction using a new level set formulation. In: Proceedings of the International Conference on Medical Image Computing and Computer Assisted Intervention. Springer Berlin Heidelberg, pp. 389–397.

Kern, M.J., Lerman, A., Bech, J.-W., De Bruyne, B., Eeckhout, E., Fearon, W.F., Higano, S.T., Lim, M.J., Meuwissen, M., Piek, J.J., Pijls, N.H.J., Siebes, M., Spaan, J.A.E., 2006. Physiological assessment of coronary artery disease in the cardiac catheterization laboratory: a scientific statement from the American Heart Association Committee on Diagnostic and Interventional Cardiac Catheterization, Council on Clinical Cardiology.. Circulation 114 (12), 1321–1341.

Klein, A.J., Garcia, J.A., Hudson, P.A., Kim, M.S., Messenger, J.C., Casserly, I.P., Wink, O., Hattler, B., Tsai, T.T., Chen, S.Y.J., Hansgen, A., Carroll, J.D., 2011. Safety and efficacy of dual-axis rotational coronary angiography vs. standard coronary angiography. Catheter. Cardiovasc. Interv. 77 (6), 820–827.

Klein, A.J.P., Garcia, J.A., 2009. Rotational coronary angiography.. Cardiol. Clin. 27 (3), 395–405.

Koppe, R., Klotz, E., Beek, J.D., Aerts, H., 1995. 3D vessel reconstruction based on rotational angiography. In: Proceedings of the Computer Assisted Radiology and Surgery, pp. 17–22.

Langan, D.A., Claus, B.E.H., Al Assad, O., Trousset, Y., Riddell, C., Avignon, G., Solomon, S.B., Lai, H., Wang, X., 2015. Interventional C-arm tomosynthesis for vascular imaging: initial results. In: Proceedings of the SPIE.. SPIE.94125N–94125N–8

Lansky, A.J., Pietras, C., 2014. Fractional flow reserve from 3-dimensional quantitative coronary angiography: fresh light through an old window.. JACC. Cardiovasc. Interv. 7 (7), 778–780.

Larrabide, I., Kim, M., Augsburger, L., Villa-Uriol, M.C., Rüfenacht, D., Frangi, A.F., 2012. Fast virtual deployment of self-expandable stents: method and in vitro evaluation for intracranial aneurysmal stenting.. Med. Image Anal. 16 (3), 721–730.

Law, A., Chan, F., 2003. 3D reconstruction of coronary artery using biplane angiography. In: Proceedings of the IEEE Engineering in Medicine and Biology Society. IEEE, pp. 533–536.

Lee, J., Chang, S., Kim, S., Lee, Y., Ryu, J., Choi, J., Kim, K., Park, J., 2012. Assessment of three dimensional quantitative coronary analysis by using rotational angiography for measurement of vessel length and diameter. Int. J. Cardiovasc. Imaging 28 (7), 1627–1634.

Lehmann, G.C., Holdsworth, D.W., Drangova, M., 2006. Angle-independent measure of motion for image-based gating in 3D coronary angiography.. Med. Phys. 33 (5), 1311–1320.

Li, J., Cohen, L.D., 2011. Reconstruction of 3D tubular structures from cone-beam projections. In: Proceedings of the IEEE International Symposium on Biomedical Imaging. IEEE, pp. 1162–1166.

Li, M., Kudo, H., Hu, J., Johnson, R.H., 2004. Improved iterative algorithm for sparse object reconstruction and its performance evaluation with micro-CT data. IEEE Trans. Nucl. Sci. 51 (3), 659–666.

Li, M., Yang, H., Kudo, H., 2002. An accurate iterative reconstruction algorithm for sparse objects: application to 3D blood vessel reconstruction from a limited number of projections. Phys. Med. Biol. 47 (15), 2599–2609.

Liao, R., Luc, D., Sun, Y., Kirchberg, K., 2010. 3-D reconstruction of the coronary artery tree from multiple views of a rotational X-ray angiography. Int. J. Cardiovasc. Imaging 26 (7), 733–749.

Ligthart, J., Witberg, K., Karanasos, A., Tu, S., Reiber, J., 2014. Can co-registration influence the accuracy of stent placement? A retrospective observational study. In: Wijns, W., Fajadet, J., Serruys, P.W. (Eds.), In: EUROPCR.

Liu, B., Zhou, F., Bai, X., 2014a. Improved C-arm cardiac cone beam CT based on alternate reconstruction and segmentation. Biomed. Signal Process. Control 13, 113–122.

Liu, X., Hou, F., Hao, A., Qin, H., 2014b. A parallelized 4D reconstruction algorithm for vascular structures and motions based on energy optimization. Vis. Comput. 31 (11), 1431–1446.

Lorenz, C., von Berg, J., Bulow, T., Renisch, S., Wergandt, S., 2004. Modeling the coronary artery tree. In: Proceedings of the International Conference on Shape Modeling and Applications. IEEE, pp. 354–399.

Mark, D.B., Berman, D.S., Budoff, M.J., Carr, J.J., Gerber, T.C., Hecht, H.S., Hlatky, M.A., Hodgson, J.M., Lauer, M.S., Miller, J.M., Morin, R.L., Mukherjee, D., Poon, M., Rubin, G.D., Schwartz, R.S., 2010. ACCF/ACR/AHA/NASCI/SAIP/SCAI/SCCT 2010 expert consensus document on coronary computed tomographic angiography: a report of the American College of Cardiology Foundation Task Force on Expert Consensus Documents.. J. Am. Coll. Cardiol. 55 (23), 2663–2699.

Mauri, L., O'Malley, A.J., Popma, J.J., Moses, J.W., Leon, M.B., Holmes, D.R., Teirstein, P.S., Cutlip, D.E., Donahoe, D., Kuntz, R.E., 2005. Comparison of thrombosis and restenosis risk from stent length of sirolimus-eluting stents versus bare metal stents.. Am. J. Cardiol. 95 (10), 1140–1145.

McCullough, P.A., 2008. Contrast-induced acute kidney injury.. J. Am. Coll. Cardiol. 51 (15), 1419–1428.

Meerkin, D., Marom, H., Cohen-Biton, O., Einav, S., 2010. Three-dimensional vessel analyses provide more accurate length estimations than the gold standard QCA. J. Interv. Cardiol. 23 (2), 152–159.

Messenger, J.C., Casserly, I.P., 2009. Advances in contrast media and contrast injectors.. Cardiol. Clin. 27 (3), 407–415.

Moreno, R., Fernández, C., Hernández, R., Alfonso, F., Angiolillo, D.J., Sabaté, M., Escaned, J., Bañuelos, C., Fernández-Ortiz, A., Macaya, C., 2005. Drug-eluting stent thrombosis: results from a pooled analysis including 10 randomized studies.. J. Am. Coll. Cardiol. 45 (6), 954–959.

Morris, P.D., Ryan, D., Morton, A.C., Lycett, R., Lawford, P.V., Hose, D.R., Gunn, J.P., 2013. Virtual fractional flow reserve from coronary angiography: modeling the significance of coronary lesions: results from the VIRTU-1 (VIRTUal Fractional Flow Reserve From Coronary Angiography) study.. JACC. Cardiovasc. Interv. 6 (2), 149–157.

Morris, P.D., van de Vosse, F.N., Lawford, P.V., Hose, D.R., Gunn, J.P., 2015. "Virtual" (computed) fractionalflowreserve: current challenges and limitations.. JACC. Cardiovasc. Interv. 8 (8), 1009–1017.

Mourgues, F., Devernay, F., Malandain, G., Coste-Manière, E., 2001. 3D+t modeling of coronary artery tree from standard non simultaneous angiograms. In: Proceedings of the International Conference on Medical Image Computing and Computer Assisted Intervention.. Springer Berlin Heidelberg, pp. 1320–1322.

Movassaghi, B., Grass, M., Schaefer, D., Rasche, V., Wink, O., Schoonenberg, G., Chen, J.Y., Garcia, J.A., Groves, B.M., Messenger, J.C., Carroll, J.D., 2007. 4D coronary artery reconstruction based on retrospectively gated rotational angiography: first in-human results. In: Proceedings of the SPIE. SPIE.65090P–65090P–6

Movassaghi, B., Rasche, V., Florent, R., Viergever, M., Niessen, W., 2003. 3D coronary reconstruction from calibrated motion-compensated 2D projections. In: Proceedings of the Computer Assisted Radiology and Surgery, vol. 1256, pp. 1079–1084.

Movassaghi, B., Rasche, V., Grass, M., Viergever, M.A., Niessen, W.J., 2004. A quantitative analysis of 3-D coronary modeling from two or more projection images.. IEEE Trans. Med. Imaging 23 (12), 1517–1531.

Neubauer, A.M., Garcia, J.A., Messenger, J.C., Hansis, E., Kim, M.S., Klein, A.J., Schoonenberg, G.A., Grass, M., Carroll, J.D., 2010. Clinical feasibility of a fully automated 3D reconstruction of rotational coronary X-Ray angiograms. Circ. Cardiovasc. Interv. 3 (1), 71–79.

Nichols, M., Townsend, N., Scarborough, P., Rayner, M., 2013. Cardiovascular disease in Europe: epidemiological update.. Eur. Heart J. 34 (39), 3028–3034.

Pantos, I., Efstathopoulos, E.P., Katritsis, D.G., 2009. Two and three-dimensional quantitative coronary angiography.. Cardiol. Clin. 27 (3), 491–502.

Papafaklis, M.I., Muramatsu, T., Ishibashi, Y., Lakkas, L.S., Nakatani, S., Bourantas, C.V., Ligthart, J., Onuma, Y., Echavarria-Pinto, M., Tsirka, G., Kotsia, A., Nikas, D.N., Mogabgab, O., van Geuns, R.-J., Naka, K.K., Fotiadis, D.I., Brilakis, E.S., Garcia–Garcia, H.M., Escaned, J., Zijlstra, F., Michalis, L.K., Serruys, P.W., 2014. Fast virtual functional assessment of intermediate coronary lesions using routine angiographic data and blood flow simulation in humans: comparison with pressure wire - fractional flow reserve.. EuroIntervention 10 (5), 574–583.

de Pierro, A.R., Beleza Yamagishi, M.E., 2001. Fast EM-like methods for maximum "a posteriori" estimates in emission tomography.. IEEE Trans. Med. Imaging 20 (4), 280–288.

Pijls, N.H.J., van Schaardenburgh, P., Manoharan, G., Boersma, E., Bech, J.-W., van't Veer, M., Bär, F., Hoorntje, J., Koolen, J., Wijns, W., de Bruyne, B., 2007. Percutaneous coronary intervention of functionally nonsignificant stenosis: 5-year follow-up of the DEFER Study.. J. Am. Coll. Cardiol. 49 (21), 2105–2111.

Radiology Support Devices, 2006. Lung/Chest Phantom.

Rasche, V., Mansour, M., Reddy, V., Singh, J., Qureshi, A., Manzke, R., Sokka, S., Ruskin, J., 2008. Fusion of three-dimensional X-ray angiography and three-dimensional echocardiography. Int. J. Comput. Assist. Radiol. Surg. 2 (5), 293–303.

Rasche, V., Movassaghi, B., Grass, M., 2004. Automatic gating window selection for gated three-dimensional coronary X-ray angiography. In: Proceedings of the Computer Assisted Radiology and Surgery, vol. 1268, pp. 1050–1054.

Rasche, V., Movassaghi, B., Grass, M., Schäfer, D., Buecker, A., 2006a. Automatic selection of the optimal cardiac phase for gated three-dimensional coronary x-ray angiography.. Acad. Radiol. 13 (5), 630–640.

Rasche, V., Movassaghi, B., Grass, M., Schäfer, D., Kühl, H.P., Günther, R.W., Bücker, A., 2006b. Three-dimensional X-ray coronary angiography in the porcine model: A feasibility study.. Acad. Radiol. 13 (5), 644–651.

Reiber, J.H.C., Tu, S., Tuinenburg, J.C., Koning, G., Janssen, J.P., Dijkstra, J., 2011. QCA, IVUS and OCT in interventional cardiology in 2011.. Cardiovasc. Diagn. Ther. 1 (1), 57–70.

Rivest-Hénault, D., Sundar, H., Cheriet, M., 2012. Nonrigid 2D/3D registration of coronary artery models with live fluoroscopy for guidance of cardiac interventions.. IEEE Trans. Med. Imaging 31 (8), 1557–1572.

Rohkohl, C., Lauritsch, G., Biller, L., Hornegger, J., 2010a. ECG-gated interventional cardiac reconstruction for non-periodic motion. In: Proceedings of the Medical Image Computing and Computer-Assisted Intervention. Springer Berlin Heidelberg, pp. 151–158.

Rohkohl, C., Lauritsch, G., Biller, L., Prümmer, M., Boese, J., Hornegger, J., 2010b. Interventional 4D motion estimation and reconstruction of cardiac vasculature without motion periodicity assumption.. Med. Image Anal. 14 (5), 687–694.

Rohkohl, C., Lauritsch, G., Keil, A., Hornegger, J., 2010c. CAVAREV–an open platform for evaluating 3D and 4D cardiac vasculature reconstruction.. Phys. Med. Biol. 55 (10), 2905–2915.

Rohkohl, C., Lauritsch, G., Nottling, A., Prummer, M., Hornegger, J., 2008a. C-arm CT: Reconstruction of dynamic high contrast objects applied to the coronary sinus. In: Proceedings of the IEEE Nuclear Science Symposium Conference Record. IEEE, pp. 5113–5120.

Rohkohl, C., Lauritsch, G., Prümmer, M., Boese, J., Hornegger, J., 2009a. Towards 4-D cardiac reconstruction without ECG and motion periodicity using C-arm CT. In: Proceedings of the International Meeting on Fully Three-Dimensional Image Reconstruction in Radiology and Nuclear Medicine, pp. 323–326.

Rohkohl, C., Lauritsch, G., Prümmer, M., Hornegger, J., 2009b. Interventional 4-D motion estimation and reconstruction of cardiac vasculature without motion periodicity assumption. In: Proceedings of the Medical Image Computing and Computer-Assisted Intervention.. Springer Berlin Heidelberg, pp. 132–139.

Rohkohl, C., Prümmer, M., Fahrig, R., Lauritsch, G., Hornegger, J., 2008b. Cardiac C-arm CT: image-based gating. In: Proceedings of the SPIE, vol. 6913.69131G–69131G–12

Rougée, A., Picard, C., Saint-Félix, D., Trousset, Y., Moll, T., Amiel, M., 1994. Three-dimensional coronary arteriography. Int. J. Card. Imaging 10 (1), 67–70.

Sakoe, H., Chiba, S., 1978. Dynamic programming algorithm optimization for spoken word recognition. IEEE Trans. Acoust. 26 (1), 43–49.

Sarry, L., Boire, J.Y., 2001. Three-dimensional tracking of coronary arteries from biplane angiographic sequences using parametrically deformable models.. IEEE Trans. Med. Imaging 20 (12), 1341–1351.

Scanlon, P.J., Faxon, D.P., Audet, A.-M., Carabello, B., Dehmer, G.J., Eagle, K.A., Legako, R.D., Leon, D.F., Murray, J.A., Nissen, S.E., Pepine, C.J., Watson, R.M., Ritchie, J.L., Gibbons, R.J., Cheitlin, M.D., Gardner, T.J., Garson, A., Russell, R.O., Ryan, T.J., Smith, S.C., 1999. ACC/AHA guidelines for coronary angiography: Executive summary and recommendations : A report of the American College of Cardiology/American Heart Association Task Force on Practice Guidelines (Committee on Coronary Angiography) Developed in collaboration. Circulation 99 (17), 2345–2357.

Schäfer, D., Borgert, J., Rasche, V., Grass, M., 2006. Motion-compensated and gated cone beam filtered back-projection for 3-D rotational X-ray angiography. IEEE Trans. Med. Imaging 25 (7), 898–906.

Schoonenberg, G., Neubauer, A., Grass, M., 2009a. Three-dimensional coronary visualization, Part 2: 3D reconstruction.. Cardiol. Clin. 27 (3), 453–465.

Schoonenberg, G.A.F., Garcia, J.A., Carroll, J.D., 2009b. Left coronary artery thrombus characterized by a fully automatic three-dimensional gated reconstruction. Catheter. Cardiovasc. Interv. 74 (1), 97–100.

Schwemmer, C., Forman, C., Wetzl, J., Maier, A., Hornegger, J., 2014. CoroEval: a multi-platform, multi-modality tool for the evaluation of 3D coronary vessel reconstructions. Phys. Med. Biol. 59 (17), 5163–5174.

Schwemmer, C., Rohkohl, C., Lauritsch, G., Müller, K., Hornegger, J., 2013a. Opening windows - increasing window size in motion-compensated ECG-gated cardiac vasculature Reconstruction. In: Qi, J., Leahy, R. (Eds.), Proceedings of the International Meeting on Fully Three-Dimensional Image Reconstruction in Radiology and Nuclear Medicine, pp. 50–53.

Schwemmer, C., Rohkohl, C., Lauritsch, G., Müller, K., Hornegger, J., 2013b. Residual motion compensation in ECG-gated interventional cardiac vasculature reconstruction. Phys. Med. Biol. 58 (11), 3717.

Segars, W.P., Sturgeon, G., Mendonca, S., Grimes, J., Tsui, B.M.W., 2010. 4D XCAT phantom for multimodality imaging research.. Med. Phys. 37 (9), 4902–4915.

Shechter, G., Devernay, F., Coste-Manière, E., Quyyumi, A., McVeigh, E.R., 2003a. Three-dimensional motion tracking of coronary arteries in biplane cineangiograms.. IEEE Trans. Med. Imaging 22 (4), 493–503.

Shechter, G., Naveh, G., Altman, A., Proksa, R.M., Grass, M., 2003b. Cardiac image reconstruction on a 16-slice CT scanner using a retrospectively ECG-gated multicycle 3D back-projection algorithm. In: Proceedings of the SPIE. SPIE, pp. 1820–1828.

Shechter, G., Resar, J.R., McVeigh, E.R., 2006. Displacement and velocity of the coronary arteries: cardiac and respiratory motion.. IEEE Trans. Med. Imaging 25 (3), 369–375.

Smith, B.D., 1985. Image reconstruction from cone-beam projections: necessary and sufficient conditions and reconstruction methods.. IEEE Trans. Med. Imaging 4 (1), 14–25.

Soille, P., 2004. Morphological Image Analysis: Principles and Applications, second ed. Springer-Verlag New York.

Sones, F.M., Shirey, E.K., 1962. Cine coronary arteriography.. Mod. Concepts Cardiovasc. Dis. 31, 735–738.

Strobel, N., Meissner, O., Boese, J., Brunner, T., Heigl, B., Hoheisel, M., Lauritsch, G., Nagel, M., Pfister, M., Rührnschopf, E.-P., Scholz, B., Schreiber, B., Spahn, M., Zellerhoff, M., Klingenbeck-Regn, K., 2009. 3D imaging with flat-detector C-Arm systems. In: Multislice CT. Springer Berlin Heidelberg. Medical Radiology, pp. 33–51.

Stuber, M., Weiss, R.G., 2007. Coronary magnetic resonance angiography. J. Magn. Reson. Imaging 26 (2), 219–234.

Szeliski, R., Zabih, R., Scharstein, D., Veksler, O., Kolmogorov, V., Agarwala, A., Tappen, M., Rother, C., 2008. A comparative study of energy minimization methods for Markov random fields with smoothness-based priors.. IEEE Trans. Pattern Anal. Mach. Intell. 30 (6), 1068–1080.

Taylor, C., Steinman, D., 2010. Image-based modeling of blood flow and vessel wall dynamics: applications, methods and future directions. Ann. Biomed. Eng. 38 (3), 1188–1203.

Tommasini, G., Camerini, A., Gatti, A., Derchi, G., Bruzzone, A., Vecchio, C., 1998. Panoramic coronary angiography. J. Am. Coll. Cardiol. 31 (4), 871–877.

Tonino, P.A.L., De Bruyne, B., Pijls, N.H.J., Siebert, U., Ikeno, F., van 't Veer, M., Klauss, V., Manoharan, G., Engstrø m, T., Oldroyd, K.G., Ver Lee, P.N., MacCarthy, P.A., Fearon, W.F., 2009. Fractional flow reserve versus angiography for guiding percutaneous coronary intervention. N. Engl. J. Med. 360 (3), 213–224.

Toutouzas, K., Chatzizisis, Y.S., Riga, M., Giannopoulos, A., Antoniadis, A.P., Tu, S., Fujino, Y., Mitsouras, D., Doulaverakis, C., Tsampoulatidis, I., Koutkias, V.G., Bouki, K., Li, Y., Chouvarda, I., Cheimariotis, G., Maglaveras, N., Kompatsiaris, I., Nakamura, S., Reiber, J.H., Rybicki, F., Karvounis, H., Stefanadis, C., Tousoulis, D., Giannoglou, G.D., 2015. Accurate and reproducible reconstruction of coronary arteries and endothelial shear stress calculation using 3D OCT: Comparative study to 3D IVUS and 3D QCA. Atherosclerosis 240 (2), 510–519.

Tsin, Y., Kirchberg, K., Lauritsch, G., Xu, C., 2009. A deformation tracking approach to 4D coronary artery tree reconstruction. In: Proceedings of the Medical Image Computing and Computer-Assisted Intervention. Springer Berlin Heidelberg, pp. 68–75.

Tu, S., Barbato, E., Köszegi, Z., Yang, J., Sun, Z., Holm, N.R., Tar, B., Li, Y., Rusinaru, D., Wijns, W., Reiber, J.H.C., 2014. Fractional flow reserve calculation from 3-dimensional quantitative coronary angiography and TIMI frame count: a fast computer model to quantify the functional significance of moderately obstructed coronary arteries.. JACC. Cardiovasc. Interv. 7 (7), 768–777.

Tu, S., Holm, N.R., Koning, G., Huang, Z., Reiber, J.H.C., 2011. Fusion of 3D QCA and IVUS/OCT.. Int. J. Cardiovasc. Imaging 27 (2), 197–207.

Tu, S., Koning, G., Jukema, W., Reiber, J.H.C., 2010. Assessment of obstruction length and optimal viewing angle from biplane X-ray angiograms.. Int. J. Cardiovasc. Imaging 26 (1), 5–17.

Tu, S., Xu, L., Ligthart, J., Xu, B., Witberg, K., Sun, Z., Koning, G., Reiber, J., Regar, E., 2012. In vivo comparison of arterial lumen dimensions assessed by co-registered three-dimensional (3D) quantitative coronary angiography, intravascular ultrasound and optical coherence tomography. Int. J. Cardiovasc. Imaging 28 (6), 1315–1327.

Tuy, H.K., 1983. An Inversion Formula for Cone-Beam Reconstruction. SIAM J. Appl. Math. 43 (3), pp.546–552.

Unberath, M., Mentl, K., Taubmann, O., Achenbach, S., Fahrig, R., Hornegger, J., Maier, A., 2015. Torsional heart motion in cone-beam computed tomography reconstruction. In: King, M., Glick, S., Mueller, K. (Eds.), Proceedings of the Internationa Meeting on Fully Three-Dimensional Image Reconstruction in Radiology Nuclear Medicine, pp. 651–654.

Unzué Vallejo, L., Delcán Domínguez, J.L., Alegría Barrero, A., Medina Peralta, J., Rodríguez Rodrigo, F.J., Rodríguez-López, J.L., 2013. Coronary lesions quantification with dual-axis rotational coronary angiography. Cardiovasc. Revascularization Med. 14 (1), 37–40.

Wahle, A., Prause, P.M., DeJong, S.C., Sonka, M., 1999. Geometrically correct 3-D reconstruction of intravascular ultrasound images by fusion with biplane angiography–methods and validation.. IEEE Trans. Med. Imaging 18 (8), 686–699.

Wiesent, K., Barth, K., Navab, N., Durlak, P., Brunner, T., Schuetz, O., Seissler, W., 2000. Enhanced 3-D-reconstruction algorithm for C-arm systems suitable for interventional procedures.. IEEE Trans. Med. Imaging 19 (5), 391–403.

Wu, H., Rohkohl, C., Hornegger, J., 2011. Total variation regularization method for 3D rotational coronary angiography. In: Proceedings of the Bild. für die Medizin. Springer Berlin Heidelberg, pp. 434–438.

Xu, C., Prince, J.L., 1998a. Generalized gradient vector flow external forces for active contours. Signal Processing 71 (2), 131–139.

Xu, C., Prince, J.L., 1998b. Snakes, shapes, and gradient vector flow.. IEEE Trans. Image Process. 7 (3), 359–369.

Xu, F., Mueller, K., 2006. A comparative study of popular interpolation and integration methods for use in computed tomography. In: Proceedings of the IEEE International Symposium Biomedical Imaging. IEEE, pp. 1252–1255.

Yang, G., Bousse, A., Toumoulin, C., Shu, H., 2007. Simulation environment for the evaluation of 3D coronary tree reconstruction algorithms in rotational angiography.. In: Proceedings of the IEEE Engineering in Medicine and Biology Society, pp. 4484–4487.

Yang, G., Hu, Y., Huang, X., Shu, H., Toumoulin, C., 2012. Simulation environment of X-ray rotational angiography using 3D+t coronary tree model.. In: Proceedings of the IEEE Engineering in Medicine and Biology Society, pp. pp.629–632.

Yang, J., Cong, W., Chen, Y., Fan, J., Liu, Y., Wang, Y., 2014. External force back-projective composition and globally deformable optimization for 3-D coronary artery reconstruction.. Phys. Med. Biol. 59 (4), 975–1003.

Yang, J., Wang, Y., Liu, Y., Tang, S., Chen, W., 2009. Novel approach for 3-d reconstruction of coronary arteries from two uncalibrated angiographic images.. IEEE Trans. Image Process. 18 (7), 1563–1572.

Zhang, J.-M., Zhong, L., Su, B., Wan, M., Yap, J.S., Tham, J.P.L., Chua, L.P., Ghista, D.N., Tan, R.S., 2014. Perspective on CFD studies of coronary artery disease lesions and hemodynamics: A review. Int. J. Numer. Method. Biomed. Eng. 30 (6), 659–680.

Zheng, S., Meiying, T., Jian, S., 2010. Sequential reconstruction of vessel skeletons from X-ray coronary angiographic sequences.. Comput. Med. Imaging Graph. 34 (5), 333–345.

Zhou, J., Bousse, A., Yang, G., Bellanger, J.-J., Luo, L., Toumoulin, C., Coatrieux, J.-L., 2008. A blob-based tomographic reconstruction of 3D coronary trees from rotational x-ray angiography. In: Proceedings of the SPIE. SPIE. pp. 69132N–69132N–12. doi: 10.1117/12.769478.

Table 1
Overview of model-based coronary artery reconstruction methods from X-ray angiography: See list of abbreviations at the bottom.

	Reference	Type	ECG	Breath-hold	Additional input	Calibration	3D reconstruction	Multi-view	Lumen surface	4D
TOP-DOWN	Sarry and Boire (2001)	BA	–	+	CLs (2)	+	Fourier deformable model with PEE	-	-	+
	Cañero et al. (2002)	BA	+	+	CLs (2)	+	ACM with PEE	-	-	-
	Zheng et al. (2010)	SA	N/A	N/A	Corresponding 2D points (2)	Opt. of ext. params	Calibration opt. followed by ACM with PEE and temporal energy	-	-	+
	Cong et al. (2015)	SA	+	N/A	CLs (2–5)	+	ACM with BPEE	+ (2–5)	+ (2–5)	-
	Yang et al. (2014)	SA	+	N/A	CLs (2)	Opt. of ext. & int. params	ACM with BPEE & calibration opt. iteratively	-	+ (N/A)	-
BOTTOM-UP	Chen and Carroll (2000)	SA	+	N/A	CLs (2)	Opt. of ext. params	Calibration opt. followed by epipolar matching + triangulation	-	+(1)	-
	Hoffmann et al. (2000)	BA	–	N/A	CLs (2)	Opt. of ext. params	Calibration opt. followed by epipolar matching + triangulation	-	-	-
	Chen and Carroll (2003)	SA	+	N/A	CLs (2)	Opt. of ext. params	Calibration opt. followed by epipolar matching + triangulation	-	+(1)	+
	Shechter et al. (2003a)	BA	–	+	CLs (2)	+	Used (Mourgues et al., 2001)	-	-	+
	Movassaghi et al. (2004)	RA	+	+	CLs (Multi, N/A)	+	Epipolar matching + triangulation	-	+ (Multi, N/A)	-
	Andriotis et al. (2008)	SA	+	N/A	Corresponding 2D points (2)	Opt. of ext. params	Calibration opt. followed by epipolar matching + triangulation	-	+ (8)	-
	Fallavollita and Cheriet (2008)	BA	–	–	CLs (2)	–	Reliable point matching & bundle adjustme, iteratively	-	-	-
	Jandt et al. (2009a)	RA	+	+	–	+	Segment from backprojected vesselness response	+ (5–9)	-	-
	Jandt et al. (2009b)	RA	+	+	–	+	Used (Jandt et al., 2009a)	+ (5–9)	+ (5–9)	+
	Yang et al. (2009)	SA	+	N/A	CLs (2)	–	Epipolar matching & bundle adjustment, iteratively	-	+(2)	-
	Liao et al. (2010)	RA	+	+	CLs (4–5)	+	Graph-cut based sparse stereo	+ (4–5)	+(1)	-
	Liu et al. (2014b)	SA	+	N/A	CLs (3)	+	Graph-cut based sparse stereo	+ (3)	-	+

List of abbreviations:
ACM = active contour model; BA = Biplane X-ray angiography; BPEE = back-projective (3D) external energy; CL = Centreline; ECG = Electrocardiogram; ext. = extrinsic; int. = intrinsic; Opt. = Optimization; param = parameter; PEE = projective (2D) external energy; RA = Rotational X-ray angiography; SA = Standard X-ray angiography; (#) = Number of X-ray images to reconstruct; N/A = not available.

Table 2
Overview of tomographic coronary artery reconstruction methods from X-ray angiography: see list of abbreviations at the bottom.

	Reference	ECG	Breath -hold	Acquisition protocol	Motion compensation			Reconstruction
					Motion model	How obtained	How applied	
GATED	Li et al. (2004)	N/A	N/A	N/A	–	–	–	TART
	Hansis et al. (2008c)	+	+	180°, 7.2 s, N/A, 30 fps	–	–	–	START
	Liu et al. (2014a)	+	N/A	180°, N/A , N/A , N/A	–	–	–	START with BR
GATED & MC	Schwemmer et al. (2013b)	+	+	N/A, 5 s, (133), N/A	2D affine and 2D B-spline	Registration between projection of initial reconstruction and projection images	Apply deformations to projection images	Artifact reduced FDK
	Hansis et al. (2010)	+	+	180°, 7.2 s, N/A, 30 fps	2D elastic warping	Registration between projection of initial reconstruction and projection images	Apply deformations to projection images	START
MC	Blondel et al. (2004)	N/A	–	120°, N/A, (100), N/A	N/A	N/A	Incorporate MVF into ART formulation	Additive Art
	Blondel et al. (2006)	-	–	200°, 5 s, N/A, 30 fps	4D B-spline	Propagation of 3D centerline construction	Incorporate MVF into ART formulation	Additive Art
	Schäfer et al. (2006)	+	+	240°, 8 s, (200), N/A	N/A	N/A	Incorporate MVF into FDK	MC FDK
	Hansis et al. (2008c)	+	+	180°, 7.2 s, N/A, 30 fps	2D elastic warping	Registration between projection of initial reconstruction and projection images	Apply deformations to projection images	FDK
	Rohkohl et al. (2010b)	+	–	200°, N/A, (133), N/A	4D B-spline	Jointly with the reconstruction	Incorporate into FDK formulation	Gradient based energy minimization

List of abbreviations:
ART = Algebraic reconstruction technique; BR = Background removal; FDK = Feldkamp–Davis–Kress algorithm; fps = frame per second; MC = Motion compensated; MVF = Motion vector field; START = Simultaneous thresholded algebraic reconstruction technique; TART = Thresholded algebraic reconstruction technique; (#) = Number of X-ray images; N/A = not available.

Table 3
Overview of evaluation types for coronary artery reconstruction from X-ray angiography methods: see list of abbreviations at the bottom.

	Reference	Hardware	Time/additional Info	Type	No	Std. of reference	Metric
Qualitative	Blondel et al. (2004)	N/A	60 min	Pat	1	N/A	N/A
	Li et al. (2004)	N/A	N/A	s - Pat	N/A - N/A	AT - AT	N/A - N/A
	Blondel et al. (2006)	N/A	40 min / 256^3	s - Pat	1 - 2	AT - AT	N/A - N/A
Quantitative: synthetic or physical phantom data	Hoffmann et al. (2000)	N/A	8–9 min	p - Pat	2 - 2	AT - AT	Inter/Intra var. - Inter/Intra var.
	Cañero et al. (2002)	N/A	N/A	s - p - Pat	1 - 1 - 5	GT, AT - N/A - N/A	Length - N/A - N/A
	Movassaghi et al. (2004)	N/A	N/A	p - A	2 - 1	GT - N/A	3D rprj - N/A
	Andriotis et al. (2008)	N/A	N/A	s	10	GT	3D rprj, Angle
	Jandt et al. (2009b)	N/A	N/A	s - p - A - Pat	1 - 1 - 1 - 2	GT - GT - N/A - N/A	3D rprj - Radius - N/A - N/A
	Schäfer et al. (2006)	3.2GHz AMD Opteron, 8GB	7–80.7 min / 256^3-512^3	s	1	GT	Voxel err. near CL
	Hansis et al. (2008d)	2.8GHz AMD Opteron, N/A	5.4–57.9 min / 0-60% gating window	s - Pat	1 - 15	GT - N/A	Radius, Energy inside GT - N/A
	Hansis et al. (2008c)	N/A	N/A	s - Pat	1 - 3	GT - N/A	Radius, Energy inside GT, Stenosis degree - N/A
	Hansis et al. (2010)	N/A	N/A	s - Pat	1 - 4	GT - AT	RRE, Total voxel err., Voxel err. near CL - N/A
	Rohkohl et al. (2010b)	NVIDIA Quadro FX 5800	3 min / 256^3	s - p - Pat	1 - 1 - 3	GT - GT - AT	Radius - Radius - N/A
	Schwemmer et al. (2013b)	2.53GHz Intel Xeon E5540, 16GB NVIDIA Quadro FX 5800 GPU	N/A	s - Pat	1 - 6	GT; AT - AT	MMO; N/A - Noise level, VS
	Liu et al. (2014a)	Intel i5-3210	218-350 s / $\sim 256^3$	s	1	GT; AT	MMO, RRE; N/A
Quantitative: real patient data	Chen and Carroll (2000)	Indigo2 R10000, 128MB	$<$ 10 min	p - Pat	1 - 40	GT - GT	Length - 2D rprj
	Sarry and Boire (2001)	1.2GHz AMD Athlon, 256MB	5 s	Pat	14	GT	2D rprj
	Chen and Carroll (2003)	Indigo2	1.0 min	s - p - Pat	N/A - N/A - 40	GT - GT - GT	Curvature, Torsion - Length, Angle - 2D rprj
	Shechter et al. (2003a)	0.75-1GHz Intel Pentium III	155 min / per cardiac phase	p - Pat	1 - 5	GT - GT	3D rprj - 2D rprj
	Fallavollita and Cheriet (2008)	N/A	N/A	s - Pat	2 - 2	GT - GT	2D, 3D rprj - 2D rprj
	Yang et al. (2009)	3.2GHz Pentium IV, 1GB	4.1–9.6 s	p - Pat	1 - 5	GT - GT	3D rprj, Radius - 2D rprj
	Jandt et al. (2009a)	AMD Opteron 2220	4 s	s - Pat	1 - 17	GT - ES(6)	3D rprj - N/A
	Zheng et al. (2010)	AMD Athlon X2 4000+, 1GB	0.21 min / per cardiac phase	Pat	5	GT	2D rprj
	Liao et al. (2010)	2.13GHz Intel Pentium M	12 s	p - A - Pat	1 - 1 - 11	GT - GT - GT	2D, 3D rprj - 2D rprj - 2D rprj
	Cong et al. (2015)	Intel i7-2600, 16G	N/A	s - Pat	1 - 6	GT - GT	2D, 3D rprj - 2D rprj
	Yang et al. (2014)	Intel i7-2600, 16G	N/A	s - Pat	6 - 8	GT - GT	2D, 3D rprj - 2D rprj
	Liu et al. (2014b)	3.4GHz Intel i7-3770, 8GB NVIDIA GTX-780 GPU	3 s	s - Pat	1 - 7	GT - GT	2D rprj - 2D rprj

List of abbreviations:
A = Animal data; AT = Alternative technique; err. = error; ES(#) = Expert score, # experts; GT = Ground truth; MMO = Maximum mean overlap; p = Physical phantom; Pat = Patient data; RRE = relative radius error; s = Software phantom; VS = Vessel sharpness; 2D rprj = 2D reprojection error; 3D rprj = 3D reprojection error; N/A = not applicable/available.